# New tools and insights in physiology and chromosome dynamics of Clostridioides difficile

Oliveira Paiva, A.M.

CHAPTER 5

# The bacterial chromatin protein HupA can remodel DNA and associates with the nucleoid in *Clostridioides difficile*

Ana M. Oliveira Paiva[1,2]

Annemieke H. Friggen[1,2]

Liang Qin[2,3]

Roxanne Douwes[1]

Remus T. Dame[2,3]

Wiep Klaas Smits[1,2]

[1] Department of Medical Microbiology, Section Experimental Bacteriology, Leiden University Medical Center, Leiden, The Netherlands

[2] Center for Microbial Cell Biology, Leiden, The Netherlands

[3] Faculty of Science, Leiden Institute of Chemistry, Leiden University, Leiden, Netherlands

Published in Journal of Molecular Biology

DOI: 10.1016/j.jmb.2019.01.001

## Abstract

The maintenance and organization of the chromosome plays an important role in the development and survival of bacteria. Bacterial chromatin proteins are architectural proteins that bind DNA, modulate its conformation and by doing so affect a variety of cellular processes. No bacterial chromatin proteins of *C. difficile* have been characterized to date.

Here, we investigate aspects of the *C. difficile* HupA protein, a homologue of the histone-like HU proteins of *Escherichia coli*. HupA is a 10 kDa protein that is present as a homodimer *in vitro* and self-interacts *in vivo*. HupA co-localizes with the nucleoid of *C. difficile*. It binds to the DNA without a preference for the DNA G+C content. Upon DNA binding, HupA induces a conformational change in the substrate DNA *in vitro* and leads to compaction of the chromosome *in vivo*.

The present study is the first to characterize a bacterial chromatin protein in *C. difficile* and opens the way to study the role of chromosomal organization in DNA metabolism and on other cellular processes in this organism.

## Introduction

*Clostridioides difficile* (also known as *Clostridium difficile*) [1] is a gram-positive anaerobic bacterium that can be found in the environment like the soil, water, and even meat products [2,3]. It is an opportunistic pathogen and the leading cause of antibiotic-associated diarrhoea in nosocomial infections [4]. *Clostridioides difficile* infection (CDI) can present symptoms that range from mild diarrhoea to more severe disease, such as pseudomembranous colitis, and can even result in death [4]. Over the past two decades the incidence of CDI worldwide, in a healthcare setting as well as in the community has increased [4-6]. *C. difficile* is resistant to a broad range of antibiotics and recent studies have reported cases of decreased susceptibility of *C. difficile* to some of the available antimicrobial therapies [7,8]. Consequently, the interest in the physiology of the bacterium has increased in order to explore new potential targets for intervention.

The maintenance and organization of the chromosome plays an important role in the development and survival of bacteria. Several proteins involved in the maintenance and organization of the chromosome have been explored as potential drug targets [9-11]. The bacterial nucleoid is a highly dynamic structure organized by factors such as the DNA supercoiling induced by the action of topoisomerases [12], macromolecular crowding [13,14] and interactions with nucleoid-associated proteins (NAPs) [15,16]. Bacterial NAPs have been implicated in efficiently compacting the nucleoid while supporting the regulation of specific genes for the proliferation and maintenance of the cell [16].

NAPs are present across all bacteria and several major families have been identified [16,17]. Some of the most abundant NAPs in the bacterial cell are bacterial chromatin proteins like the histone-like HU/IHF protein family [18,19]. *Escherichia coli* contains three HU/IHF family proteins (αHU, βHU, IHF) that have been extensively characterized [19-22]. By contrast, *Bacillus subtilis* and several other gram-positive organisms only contain one protein of the HU/IHF protein family [17,19,23]. In *E. coli* disruption of αHU and/or βHU function leads to a variety of growth defects or sensitivity to adverse conditions, but HU is not essential for cell survival [24,25]. However, in *B. subtilis* the HU protein HBsu is essential for cell viability, likely due to the lack of functional redundancy of the HU proteins such as in *E. coli* [17,23].

In solution, most HU proteins are found as homodimers or heterodimers and are able to bind DNA through a flexible DNA binding domain. The crystal structure of the *E. coli* αHU-βHU heterodimer suggests the formation of higher-order complexes at higher protein concentrations [22]. Modelling of these complexes suggests HU proteins have the ability to form

higher-order complexes through dimer-dimer interaction and make nucleoprotein filaments [22,26,27]. However, the physiological relevance of these is still unclear [18,22,27].

The flexible nature of the DNA-binding domain in HU proteins confers the ability to accommodate diverse substrates. Most proteins bind with variable affinity and without strong sequence specificity to both DNA and RNA [28]. Some bacterial chromatin proteins have a clear preference for AT-rich regions [29-31] or for the presence of different structures on the DNA [28,32].

HU proteins can modulate DNA topology in various ways. They can stabilize negatively supercoiled DNA or constrain negative supercoils in the presence of topoisomerase [22,33]. HU proteins are involved in modulation of the chromosome conformation and have been shown to compact DNA [16,26,34]. This compaction of DNA is possible through the ability of HU proteins to introduce flexible hinges and/or bend the DNA [16,26,34,35].

The ability to induce conformational changes in the DNA influences a variety of cellular processes due to an indirect effect on global gene expression [36-40]. In *E. coli* HU proteins are differentially expressed during the cell cycle. The αHU-βHU heterodimer is prevalent in stationary phase, while during exponential growth HU is predominantly present as homodimers [21]. Several studies suggest an active role of HU proteins in the transcription and translation of other proteins and even on DNA replication and segregation of the nucleoids [41-43].

The diverse roles of HU proteins are underscored by their importance for metabolism and virulence in bacterial pathogens. Disruption of both HU homologues (αHU and βHU) in *Salmonella typhimurium*, for example, results in the down-regulation of the pathogenicity island SPI2 and consequently a reduced ability to survive during macrophage invasion [44]. Other studies have shown the importance of HU proteins for the adaptation to stress conditions, such as low pH or antibiotic treatment [45-47]. For instance, in *M. smegmatis* deletion of *hupB* leads to increased sensitivity to antimicrobial compound [46].

Despite the wealth of information from other organisms, no bacterial chromatin protein has been characterized to date in the gram-positive enteropathogen *Clostridioides difficile*. In this study, we show that *C. difficile* HupA (CD3496) is a legitimate homologue of the bacterial HU proteins. We show that HupA exists as a homodimer, binds to DNA and co-localizes with the nucleoid. HupA binding induces a conformational change of the substrate DNA and leads to compaction of the chromosome. This study is the first to characterize a bacterial chromatin protein in *C. difficile*.

## Results and Discussion

### *C. difficile* encodes a single HU protein, HupA

To identify bacterial chromatin proteins in *C. difficile*, we searched the genome sequence of *C. difficile* for homologues of characterized HU proteins from other organisms. Using BLASTP (https://blast.ncbi.nlm.nih.gov/), we identified a single homologue of the HU proteins in the genome of the reference strain 630 [48]; GenBank: AM180355.1), encoded by the *hupA* gene (CD3496)(e-value: 1e-22). This is similar to other gram-positive organisms, where also a single member of this family is found [17,19,23] and implies an essential role of this protein on the genome organization in *C. difficile*. Moreover, lack of *hupA* mutants during random transposon mutagenesis of the epidemic *C. difficile* strain R20291 supports that the *hupA* gene (CDR20291_3333) is essential [49].

Alignment of HupA amino acid sequence with selected homologues from other organisms show a sequence identity varying between 58% to 38% (Fig. 1A). HupA displays the highest sequence identity with *Staphylococcus aureus* HU (58%). When compared to the *E. coli* HU proteins, HupA has higher sequence identity with βHU (47%) than with αHU (43%).

The overall structure of HU proteins is conserved has previously described by the analysis of several nucleoid-associated proteins [19,50]. To confirm the structural similarity of the *C. difficile* HupA protein to other HU proteins, we performed a PHYRE2 structure prediction [51]. All top-scoring models are based on structures from the HU family. The model with the highest confidence (99.9) and largest % identity (60%) is based on a structure of the *S. aureus* HU protein (PDB: 4QJU). Next, we generated a structural model of HupA using SWISS-MODEL [52] and *S. aureus* HU protein (Uniprot ID: Q99U17) [53] as a template. As expected, the predicted structure (Fig. 1B) is a homodimer, in which each monomer contains two domains as is common for HU proteins [50,53]. The α-helical dimerization domain contains a helix-turn-helix (HTH) and the DNA-binding domain consists of a protruding arm composed of 3 β-sheets (Fig. 1B). In the dimer, the two β-arms form a conserved pocket that can extensively interact with the DNA [53] (Fig 1).

Crystal structures of HU-DNA complexes have shed light on the mode of interaction of HU proteins with DNA and an overall mechanism for DNA binding has been proposed [35,53-55]. In the co-crystal structure of *S. aureus* HU the arms embrace the minor groove of the dsDNA [53]. Proline residues at the terminus of the arms cause distortion of the DNA helix, by creating or stabilizing kinks [35,53]. Further electrostatic interactions between the sides of HU dimers and the phosphate backbone facilitate DNA bending [56]. In *Borrelia burgdorferi* direct interactions

between the DNA backbone and the helices of the Hbb protein dimerization domain were observed [55]. The overall similarity of *C. difficile* HupA to other HU family proteins (Fig. 1A) and a similar predicted electrostatic surface potential (Fig. 1C) suggest a conserved mechanism on HupA DNA binding in *C. difficile*.

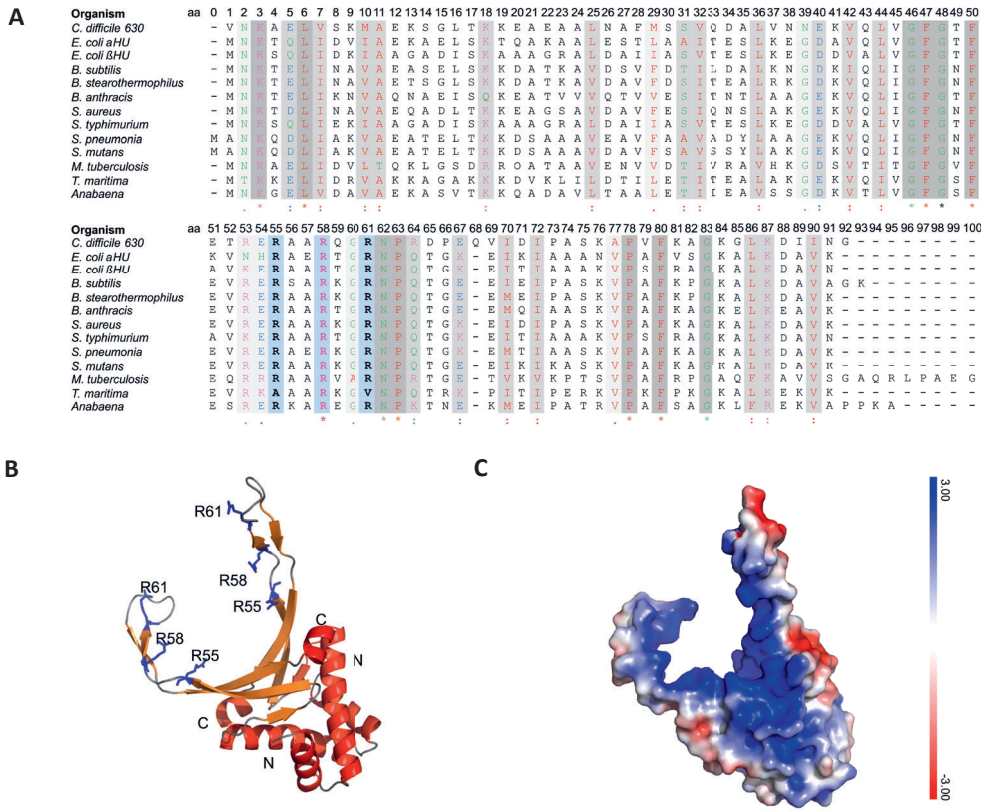


**Fig. 1 - *C. difficile* HupA is a homologue of bacterial HU proteins. A)** Multiple sequence alignment (ClustalOmega) of *C. difficile* HupA with homologous proteins from the Uniprot database. The protein sequences from *C. difficile* 630Δ*erm* (Q180Z4), *E. coli* αHU (P0ACF0), *E. coli* βHU (P0ACF4), *B. subtilis* (A3F3E2), *G. stearothermophilus* (P0A3H0), *B. anthracis* (Q81WV7), *S. aureus* (Q99U17), *S. typhimurium* (P0A1R8), *S. pneumoniae* (AAK75224), *S. mutans* (Q9XB21), *M. tuberculosis* (P9WMK7), *T. maritima* (P36206), and *Anabaena sp*. (P05514) were selected for alignment. Residues are coloured according to ClustalW2 convention. Conserved residues (indicated with symbols below the alignment) are additionally highlighted with grey shading (darker = more conserved), except for the three arginine residues that were subjected to mutagenesis (in bold), which are highlighted in blue. **B)** Structural model of the *C. difficile* HupA dimer based on homology with the crystal structure of DNA-bound nucleoid-associated protein SAV1473 (SWISS-MODEL, PDB: 4QJN, 58.43% identity). α-Helixes are represented in red, β-sheets in orange, and unstructured regions in grey. Both the N-terminus and the C-terminus are indicated in the figure. A DNA binding pocket is formed by the arm regions of the dimer, composed of four β-sheets in each monomer. The localization of the substituted residues (R55, R58, and R61) are

indicated (blue, sticks). **C)** Electrostatic surface potential of *C. difficile* HupA. The electrostatic potential is in eV with the range shown in the corresponding colour bar.

**Mutating arginine residues in the beta-arm of HupA eliminates DNA binding**

Based on the alignment and structural model of HupA (Fig. 1) we predict that several amino acid residues in *C. difficile* HupA could be involved in the interaction with DNA. Specifically, the positively charged arginine residues R55, R58 and R61 on the β-arms of HupA (Fig. 1A and B) were of interest. In *B. stearothermophilus* arginine 55 of BstHU (residue reference to *C. difficile*) is essential for the interaction with DNA, while residues R58 and R61 have a minor effect [57]. In contrast, R58 and R61 play an important role in DNA binding of *E. coli* βHU [58]. In *S. aureus* substitutions of the residue R58, reduced the affinity of HU for DNA while R55 and R61 were crucial for proper DNA binding [53].

As it has been shown that disruption of a single residue may not be sufficient to abolish DNA binding [32,57,58], we substituted the residues R55, R58 and R61 (Fig. 1B, blue sticks) in *C. difficile* HupA based on the published mutations in HU from other organisms [53,57,58]. Residue R55 was changed to glutamine (Q), a neutral residue with a long side chain. R58 and R61 were replaced by glutamic acid (E) and aspartic acid (D), respectively, both negatively charged residues. The resulting protein is referred to as $HupA^{QED}$. Evaluation of the effect of these mutations on the electrostatic surface potential of the structural model of HupA reveals that compared to the wild-type protein (Fig. 1C), $HupA^{QED}$ exhibits a reduced positively charged surface of the DNA binding pocket (Fig. S1), which is expected to prevent the interaction with DNA.

To test the DNA binding of HupA and $HupA^{QED}$ we performed gel mobility shift assays. *C. difficile* HupA and $HupA^{QED}$ were heterologously produced and purified as 6x histidine-tagged fusion proteins ($HupA_{6xHis}$ and $HupA^{QED}{}_{6xHis;}$ see Materials and Methods). We incubated increasing concentrations of protein with different [ɣ-$^{32}$P]-labelled 38 bp double-stranded DNA (dsDNA) fragments with different [G+C]-content. When $HupA_{6xHis}$ was incubated with the DNA fragment a shift in mobility is evident, dependent on the protein concentration (Fig. 2A). At 2 µM of protein, approximately 70% of DNA is present as a DNA:protein complex (Fig. 2B). This clearly demonstrates that $HupA_{6xHis}$ is capable of interacting with DNA.

Some nucleoid-associated proteins demonstrate a preference for AT-rich regions [29,30,59]. We considered that binding of HupA could show preference for low G+C content DNA, since *C. difficile* has a low genomic G+C content (29.1% G+C). We tested DNA binding to dsDNA with 71.1%; 52.6% and 28.9% G+C content but observed no notable difference in the affinity (Fig. 2B). Our analyses do not exclude possible sequence preference or differential affinity for DNA with different structures (e.g. bent, looped, or otherwise deformed)[28,53].

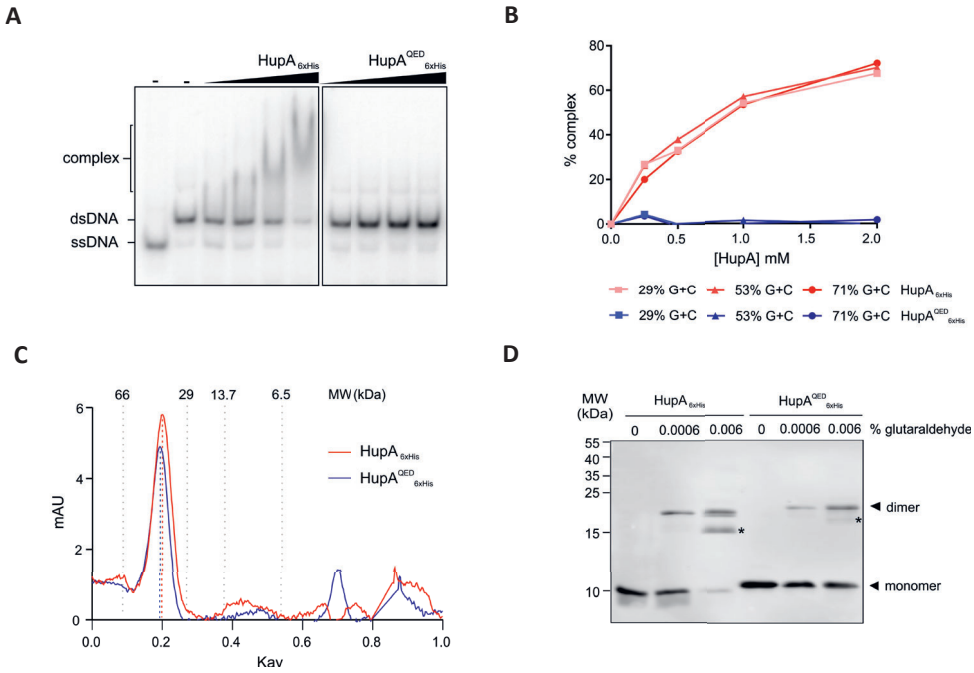


**Fig. 2 - Dimerization of HupA is independent of DNA binding. A)** Electrophoretic mobility shift assays with increasing concentrations (0.25–2 µM) of $HupA_{6xHis}$ and $HupA^{QED}{}_{6xHis}$. Gel shift assays were performed with 2.4 nM radio-labeled ([ɣ-32P] ATP) 29% G + C dsDNA oligonucleotide incubated with HupA for 20 min at room temperature prior to separation. Protein–DNA complexes were analyzed on native 8% polyacrylamide gels, vacuum-dried and visualized by phosphorimaging. ssDNA and dsDNA (without protein added, "-") were used as controls. **B)** Quantification of the gel-shift DNA–protein complex by densitometry. Gel shift assays were performed with 2.4 nM radio-labelled ([ɣ-32P] ATP) dsDNA oligonucleotides with different 29%–71% G + C content and the indicated concentration of $HupA_{6xHis}$ (red) and HupAQED 6xHis (blue). **C)** Elution profiles of $HupA_{6xHis}$ (red) and $HupA^{QED}{}_{6xHis}$ (blue) from size-exclusion chromatography. The experiments were performed with purified protein (100 µM) on a Superdex HR 75 10/30 column. The elution position of protein standards of the indicated MW (in kDa) is indicated by vertical grey dashed lines. The elution profiles show a single peak, corresponding to a ~38 kDa multimer when compared to the predicted molecular weight of the monomer (11 kDa). No significant difference in the elution profile of the $HupA^{QED}{}_{6xHis}$ compared to $HupA_{6xHis}$ was observed. **D)** Western blot analysis of glutaraldehyde cross-linking of $HupA_{6xHis}$ and $HupA^{QED}{}_{6xHis}$. HupA (100 ng) was incubated with 0%, 0.0006%, and 0.006% glutaraldehyde for 30 min at room temperature. The samples were resolved by SDS-PAGE and analyzed by immunoblotting with anti-his antibody. Crosslinking between the HupA monomers is observed with the approximate molecular weight of a homo-dimer (~22 kDa). Additional bands of lower molecular weight HupA are observed (*) that likely represent breakdown products.

Having established DNA binding by $HupA_{6xHis}$, we examined the effect of replacing the arginine residues in the β-arm in the same assay. When $HupA^{QED}{}_{6xHis}$ was incubated with all three tested DNA fragments, no shift was observed (Fig. 2A and B). This suggests that the introduction of the R55Q, R58E and R61D mutations successfully abolished binding of HupA to short dsDNA probes. We conclude that the arginine residues are crucial for the interaction with DNA and

that the DNA-binding by HupA through the protruding β-arms is consistent with DNA binding by HU homologues from other organisms [35,53,57].

**Disruption of DNA binding does not affect oligomerization**

HU proteins from various organisms have been found to form homo- or heterodimers [18,19,22,53]. To determine the oligomeric state of *C. difficile* HupA protein, we performed size exclusion chromatography [60]. The elution profile of the purified protein was compared to molecular weight standards on a Superdex 75 HR 10/30 column. Wild-type $HupA_{6xHis}$ protein exhibited a single clear peak with a partition coefficient (Kav) of 0.19 (Fig. 2C). These values correspond to an estimated molecular weight of a 38 kDa, suggesting a multimeric assembly of $HupA_{6xHis}$ (theoretical molecular weight of monomer is 11 kDa). Similar to $HupA_{6xHis}$, $HupA^{QED}_{6xHis}$ exhibits only one peak with a Kav of 0.20 and calculated molecular weight of 37 kDa (Fig. 2C). Thus, mutation of the residues in the DNA-binding pocket of HupA did not interfere with the ability of HupA to form multimers in solution.

The calculated molecular weight for both proteins is higher than we would expect for a dimer (22 kDa), by analogy with HU proteins from other organisms. However, we cannot exclude the possibility the conformation of the proteins affects the mobility in the size exclusion experiments. Therefore, to further understand the oligomeric state of HupA, we performed glutaraldehyde crosslinking experiments. HupA monomers cross-linked with glutaraldehyde were analyzed by western-blot analysis using anti-his antibodies. Upon addition of glutaraldehyde (0.0006 % and 0.006 %) we observed an additional signal around 23 kDa (Fig. 2D), consistent with a HupA dimer. No higher order oligomers were observed under the conditions tested. A similar picture was obtained for $HupA^{QED}_{6xHis}$ (Fig. 2D). Together, these experiments support the conclusion that HupA of *C. difficile* is a dimer in solution, similar to other described HU homologues, and that the ability to form dimers is independent of DNA-binding activity.

**HupA self-interacts in vivo**

Above, we have shown that HupA of *C. difficile* forms dimers *in vitro.* We wanted to confirm that the protein also self-interacts *in vivo*. We developed a split-luciferase system to allow the assessment of protein-protein interactions in *C. difficile*. Our system is based on NanoBiT (Promega) [61] and our previously published codon-optimized variant of Nanoluc, $sLuc^{opt}$ [62]. The system allows one to study protein-protein interactions *in vivo* in the native host, and thus present an advantage over heterologous systems. The large (LgBit) and small (SmBit) subunits of this system have been optimized for stability and minimal self-association by substitution

of several amino acid residues [61]. When two proteins are tagged with these subunits and interact, the subunits come close enough to form an active luciferase enzyme that is able to generate a bright luminescent signal once the substrate is added. We stepwise adapted our sLuc$^{opt}$ reporter [62] by 1) removing the signal sequence (resulting in an intracellular luciferase, Luc$^{opt}$), 2) introducing the mutations corresponding to the amino acid substitutions in NanoBiT (resulting in a full-length luciferase in which SmBiT and LgBiT are fused, bitLuc$^{opt}$) and finally, 3) the construction of a modular vector containing a polycistronic construct under the control of the anhydrotetracycline (ATc)-inducible promoter $P_{tet}$ [63] (see Supplemental Methods).

To assess the ability of HupA to form multimers *in vivo*, we genetically fused HupA to the C-terminus of both SmBit and LgBit subunits and expressed them in *C. difficile* under the control of the ATc-inducible promoter. As controls, we assessed luciferase activity in strains that express full-length luciferase (bitLuc$^{opt}$) and combinations of HupA-fusions with or without the individual complementary subunit of the split luciferase (Fig. 3). Expression of the positive control bitLuc$^{opt}$ results in a 2-log increase in luminescence signal after 1 hour of induction (1954024 ± 351395 LU/OD, Fig. 3). When both HupA-fusions are expressed from the same operon a similar increase in the luminescence signal is detected (264646 ± 122518 LU/OD at T1, Fig. 3). This signal is dependent on HupA being fused to both SmBit and LgBiT, as all negative controls demonstrate low levels of luminescence that do not significantly change upon induction (Fig. 3).

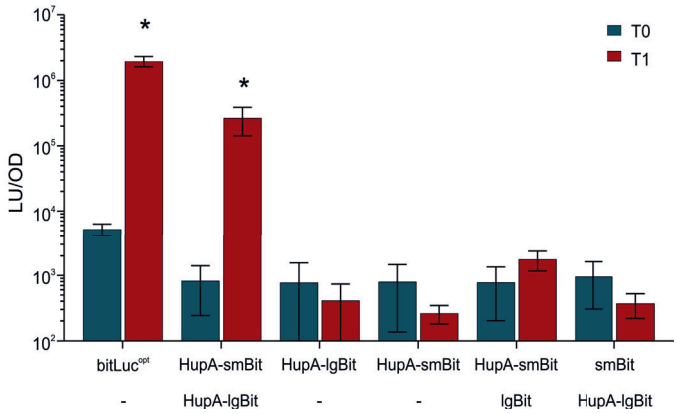


**Fig. 3 - HupA demonstrates self-interaction in *C. difficile*.** A split luciferase complementation assay was used to demonstrate interactions between HupA monomers in vivo. Cells were induced with 200 ng/mL anhydrotetracycline (ATc) for 60 min. Optical density-normalized luciferase activity (LU/OD) is shown right before induction (T0, blue bars) and after 1 h of induction (T1, red bars). The averages of biological triplicate measurements are shown, with error bars indicating the standard deviation from the mean. Luciferase activity of strains AP182 ($P_{tet}$-*bitluc$^{opt}$*), AP122 ($P_{tet}$-*hupA-smbit/hupA-lgbit*), AP152 ($P_{tet}$-*hupA-lgbit*), AP153 ($P_{tet}$-*hupA-smbit*), AP183 ($P_{tet}$-*hupA-smbit-lgbit*), and AP184 ($P_{tet}$-*smbit-hupA-lgbit*). A

positive interaction was defined on the basis of the negative controls as a luciferase activity of >1000 LU/OD. No significant difference was detected at T0. AP122 and AP182 were significantly higher with *p<0.0001 by two-way ANOVA.

Our results indicate that HupA also self-interacts *in vivo.* However, we cannot exclude that the self-interaction is mediated by other components of the cell (DNA substrate or interaction partners) that can bring HupA monomers in close proximity to each other.

**HupA overexpression leads to a condensed nucleoid**

To determine if inducible expression of HupA leads to condensation of the chromosome in *C. difficile*, we introduced a plasmid carrying *hupA* under the ATc-inducible promoter $P_{tet}$ into strain *630Δerm* [64]. This strain (AP106) also encodes the native *hupA* and induction of the plasmid-borne copy of the gene is expected to result in overproduction of HupA. AP106 cells were induced in exponential growth phase and imaged 1 hour after induction. In wild-type or non-induced AP106 cells nucleoids can be seen, after staining with DAPI stain, with a signal spread throughout most of the cytoplasm (Fig. 4A). In some cells, a defined nucleoid is observed localized near the cell centre (Fig. 4A). This heterogeneity in nucleoid morphology is likely a reflection of the asynchronous growth.

When HupA expression is not induced, the average nucleoid size is 3.10 ± 0.93 µm, similar to wild-type *C. difficile* 630Δ*erm* cells (3.32 ± 1.16 µm). Upon induction of HupA expression a significant decrease in size of the nucleoid is observed (Fig. 4A and b, white arrow). When cells are induced with 50, 100 or 200 ng/mL ATc the average nucleoid size was 1.91 ± 0.80 µm; 1.90 ± 0.82 µm and 2.02 ± 0.94 µm, respectively (Fig. 4B). No significant difference was detected between the strains induced with different ATc concentrations (Fig. 4B).

In wild-type *C. difficile* 630Δ*erm* cells the average cell length is 5.14 ± 1.09 µm, similar to non-induced AP106 cells (5.18 ± 1.09 µm, Fig. 4C). In the presence of increasing amounts of ATc a small but significant increase of cell length is observed after 1 hour induction. When cells are induced with 50, 100 or 200 ng/mL ATc the average cell length was 5.79 ± 0.80 µm; 5.58 ± 0.82 µm and 6.07 ± 0.94 µm, respectively (Fig. 4C). We did not observe an impairment of the septum formation and -localization (data not shown).

The decrease in the nucleoid size when HupA is overexpressed suggests that HupA can compact DNA *in vivo*. This observation is reminiscent of HU overexpression effects reported for other organisms, like *B. subtilis* and *Mycobacterium tuberculosis* [10,23].

### HupA co-localizes with the nucleoid

If HupA indeed exerts an influence on the nucleoid, as suggested by our experiments above, it is expected that the protein co-localizes with the DNA. To test this, we imaged HupA protein and the nucleoid in live *C. difficile*. Here, we use the HaloTag protein (Promega) [65] for imaging the subcellular localization of HupA. Tags that become fluorescent after covalently labelling by small compounds, such as HaloTag, are proven to be useful for studies in bacteria and yeast [66-68]. In contrast to GFP, does not require the presence of oxygen for maturation and should allow live-cell imaging in anaerobic bacteria.

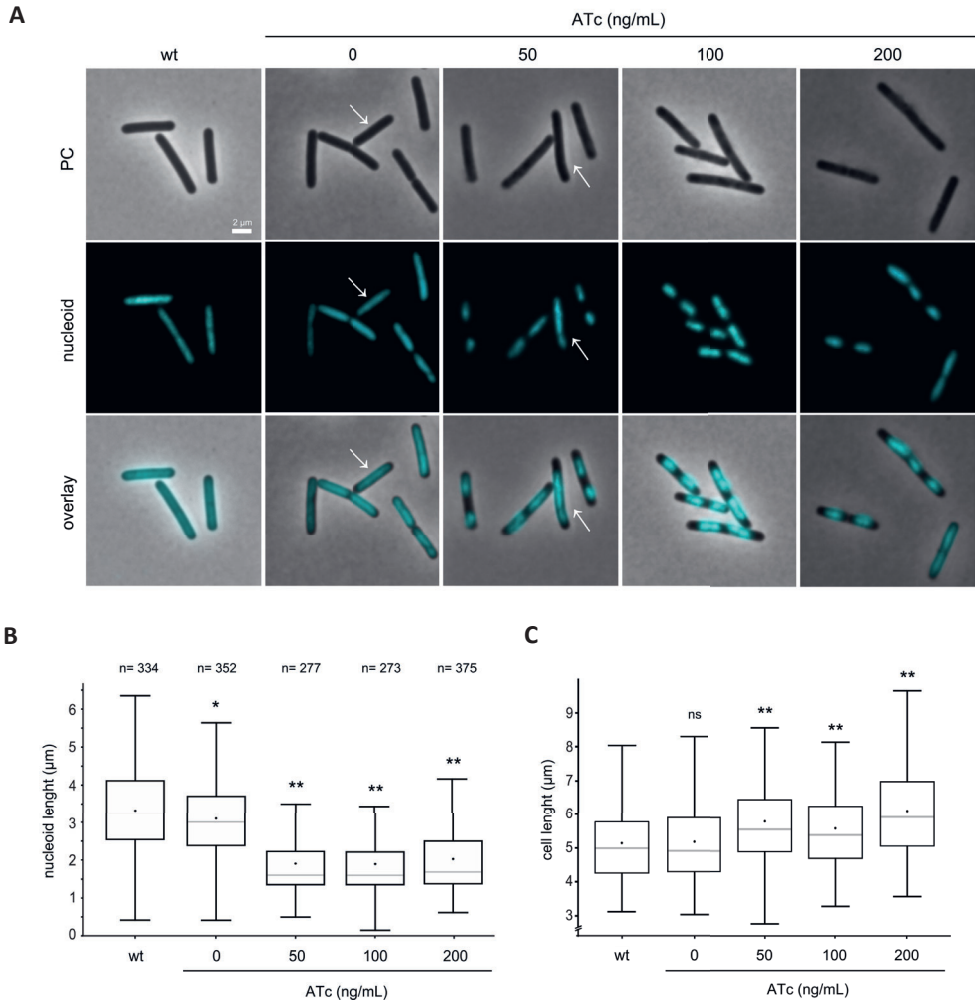


**Fig. 4 - HupA overexpression leads to compaction of the nucleoid in vivo. A)** Fluorescence microscopy analysis of *C. difficile* 630Δ*erm* harbouring the vector for anhydrotetracycline (ATc)-dependent overexpression of HupA (AP106). For HupA overexpression, cells were induced at mid-exponential

growth in liquid medium with different ATc concentrations (50, 100, and 200 ng/mL) for 1 h. C. *difficile* 630Δ*erm* and non-induced AP106 were used as controls. The cells were stained with DAPI for DNA visualization (nucleoid). The nucleoid was false coloured in cyan for better contrast. Phase contrast (PC) and an overlay of both channels are shown. Because growth is asynchronous in these conditions, cells representing different cell cycles stages can be found. In the presence of ATc, the chromosome appears more compacted. White arrow indicates the cells with mid-cell nucleoid. The scale bar represents 2 µm. **B)** Boxplots of mean nucleoid length. Whiskers represent the minimum and maximum nucleoid length observed. Black dots represent the mean values, and the grey lines represent the median values. Quantifications were performed using MicrobeJ from at least two biological replicates for each condition. n is the number of cells analyzed per condition. **C)** Boxplots of mean cell length. Whiskers represent the minimum and maximum cell length observed. Black dots represent the mean and the grey lines represent the median values. Quantifications were performed using MicrobeJ from at least two biological replicates for each condition. The same cells as analyzed for nucleoid length were used. *p< 0.05, **p<0.0001 by one-way ANOVA compared to wildtype (wt). ns = nonsignificant.

We introduced a modular plasmid expressing HupA-HaloTag from the ATc-inducible promoter $P_{tet}$ [63] into strain 630Δ*erm* [64], yielding strain RD16. Repeated attempts to create a construct that would allow us to integrate the fusion construct on the chromosome of *C. difficile* using allelic exchange failed, likely due to toxicity of the *hupA* upstream region in *E. coli* (cloning intermediate). For the visualization of HupA-HaloTag we used the Oregon green substrate, that emits at $Em_{max}$ 520 nm. Although autofluorescence of *C. difficile* has been observed at wavelengths of 500-550 nm [69,70] we observed limited to no green signal in the absence of the HaloTag (our unpublished observations and Fig. 5A, -ATc).

HupA-Halotag expression was induced in RD16 cells during exponential growth phase with 200 ng/mL ATc and cells were imaged after 1 hour of induction. In the absence of ATc, no green fluorescent signal is visible, and the nucleoid (stained with DAPI) appears extended (Fig. 5A). Upon HupA-HaloTag overexpression, the nucleoids are more defined and appear bilobed (Fig. 5A and B), similar to previous observations (Fig. 4A). The Oregon Green signal co-localizes with the nucleoid, located in the centre of the cells, with a bilobed profile that mirrors the profile of the DAPI stain (Fig. 5A and B). This co-localization is observed for individual cells at different stages of the cell cycle and is independent of the number of nucleoids present (data not shown). The localization pattern of the *C. difficile* HupA resembles that of HU proteins described in other organisms [23,71,72] (Fig 5A). Expression levels of HupA-Halotag were confirmed by SDS-PAGE in-gel fluorescence of whole-cell extracts, after incubation with Oregon Green (Fig. 5C).

ATc-induced RD16 cells exhibit a heterogeneous Oregon Green fluorescent signal. This has previously been observed with other fluorescent reporters in *C. difficile* [68-70,73] and can likely be explained by both heterogeneous expression from inducible systems [74] and different stages

of the cell cycle. For instance, the localization of cell division proteins, such as MldA or FtsZ is dependent on septum formation and thus dependent on cells undergoing cell division [69,73].

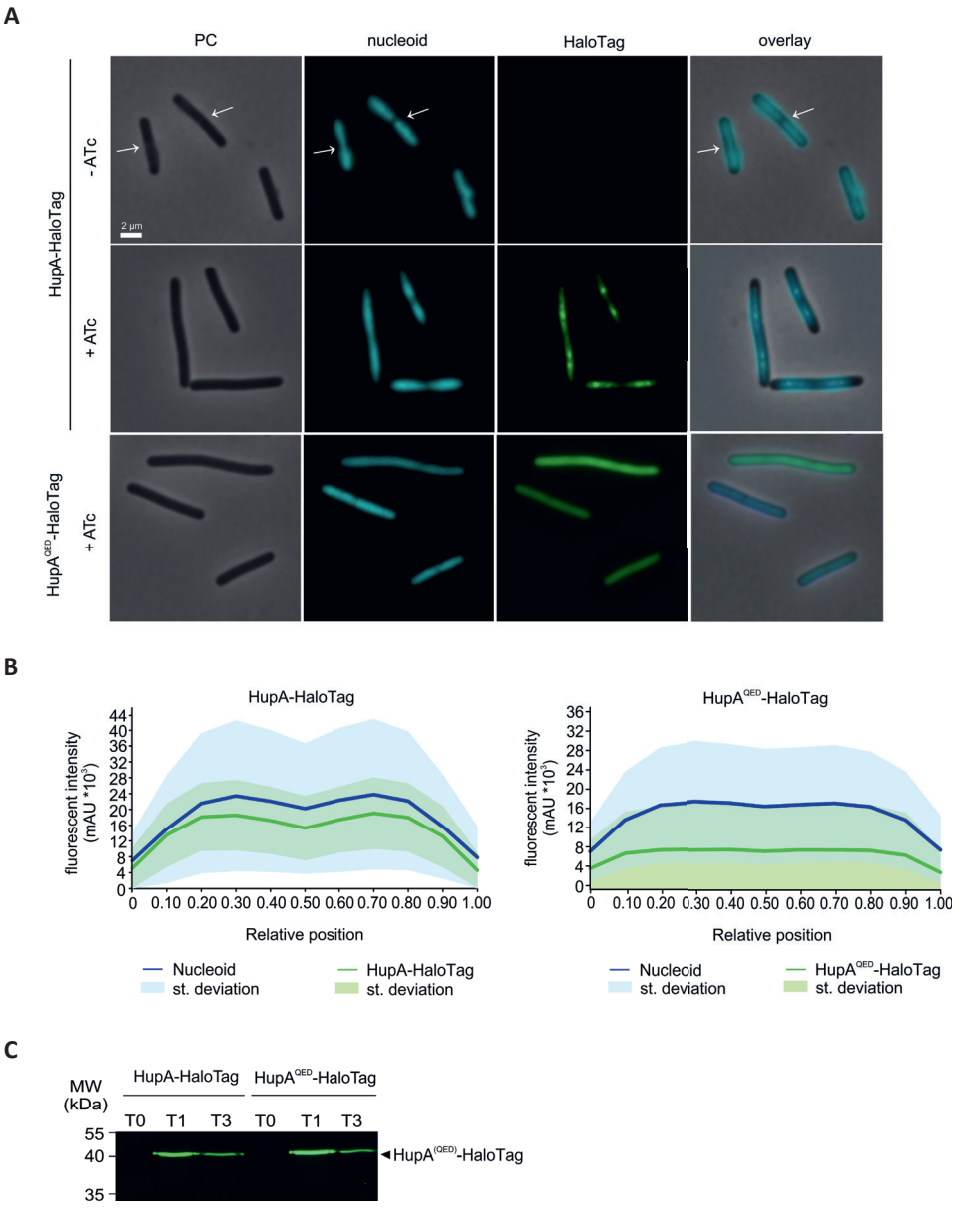


**Fig. 5 - HupA co-localizes with the nucleoid. A)** Fluorescence microscopy analysis of *C. difficile* 630Δ*erm* harbouring a vector for expression of HupA-HaloTag (RD16) or a vector for expression of HupA$^{QED}$-HaloTag (AF239). For visualization of HupA-HaloTag and HupA$^{QED}$-HaloTag, cells were induced at mid-exponential growth phase with 200 ng/mL anhydrotetracycline (ATc) for 1 h and incubated with Oregon

Green HaloTag substrate for 30 min. The cells were stained with DAPI stain to visualize DNA (nucleoid). The nucleoid was false coloured in cyan for better contrast. As control noninduced RD16 is shown, but similar results were obtained for non-induced AF239. Phase contrast (PC) and an overlay of the channels are shown. Because growth is asynchronous under these conditions, cells representing different cell cycles stages can be found. In the presence of ATc, the chromosome appears more compacted and HupA-HaloTag co-localizes with the nucleoid. The scale bar represents 2 µm. **B)** Average intensity profile scans for the nucleoid (DAPI, blue line) and HupA fusion protein (Oregon Green, green line) obtained from a MicrobeJ analysis from at least two biological replicates in each condition. Two hundred eighty-nine cells were analyzed for HupA-HaloTag, and 331 cells were analyzed for $HupA^{QED}$-HaloTag. Standard deviation of the mean is represented by the respective colour shade. **C)** In-gel fluorescent analysis of RD16 and AF239 samples before induction (T0), and 1 and 3 h after induction (T1, T3). Samples were incubated with Oregon Green substrate for 30 min and run on a 12% SDS-PAGE.

We found that $HupA^{QED}{}_{6xHis}$ does not bind dsDNA in the electrophoretic mobility shift assay (Fig. 2B). We introduced the triple substitution in the HupA-HaloTag expression plasmid to determine its effect on the localization of the protein in *C. difficile.* We found that the $HupA^{QED}$-HaloTag protein was broadly distributed throughout the cell and no compaction of the nucleoid is observed, unlike observed for ATc-induced RD16 cells (HupA-Halotag), (Fig. 5A). The lack of compaction is not due to lower expression levels of $HupA^{QED}$-Halotag, as similar levels where observed to HupA-HaloTag upon induction over time (Fig. 5C).

The nucleoid morphology upon expression of $HupA^{QED}$-HaloTag is similar to that observed in wild type 630Δ*erm* cells (Fig. 4A), suggesting that $HupA^{QED}$ does not influence the activity of the native HupA *in vivo*. Though the mutated residues did not affect oligomerization (Fig. 2C and D) we considered the possibility that $HupA^{QED}$ is unable to form heterodimers with native HupA. To evaluate whether $HupA^{QED}$ and HupA can interact, we performed glutaraldehyde crosslinking and an *in vivo* complementation assay (Fig. S2). To allow for discrimination between monomers of wild type and mutant HupA in the crosslinking assay, we purified the HupA-HaloTag from *C. difficile* and incubated this protein with heterologously produced and purified $HupA_{6xHis}$ or $HupA^{QED}{}_{6xhis}$. Upon crosslinking bands corresponding to dimers of the his-tagged (22 kDa) and the HaloTagged protein (96 kDa) are detectable (Fig. S2A), confirming our previous results (Fig. 2D). We also detect a signal corresponding to the molecular weight of a heterodimer with both $HupA_{6xhis}$ and $HupA^{QED}{}_{6xhis}$ (56 kDa), suggesting that wild type and mutant protein can form heterodimers *in vitro* (Fig S2A). To analyze the *in vivo* behaviour of these proteins, $HupA^{QED}$ was expressed fused to SmBit and HupA to LgBit in the split luciferase complementation assay. In line with the crosslinking experiment, we observe luciferase reporter activity that is similar to that observed for AP122 (HupA-SmBiT/HupA-LgBiT). Thus, mutation of the arginine residues does not abolish the self-interaction *in vivo*. Nevertheless, it is conceivable that wild type homodimers are preferentially formed *in vivo* despite the

HupA$^{QED}$ expression: the lack of DNA binding by HupA$^{QED}$ could result in a lower local concentration at the nucleoid compared to wild type HupA.

Together, these results indicate that HupA co-localizes with the nucleoid and that nucleoid compaction upon HupA overexpression is possibly dependent on its DNA-binding activity. We cannot exclude that the nucleoid compaction observed could be an indirect outcome of HupA overexpression by influencing possible interaction with the RNA and/or other proteins, or by altering transcription/translation [40,75].

**HupA compacts DNA *in vitro***

To substantiate that the decrease in nucleoid size is directly attributable to the action of HupA, we sought to demonstrate a remodelling effect of HupA on DNA *in vitro*. We performed a ligase-mediated DNA cyclization assay. Previous work has established that a length smaller than 150 bp greatly reduces the possibility of the extremities of dsDNA fragments to meet. This makes the probability to ligate into closed rings less [76]. However, in the presence of DNA bending proteins exonuclease III (ExoIII)-resistant (thus closed) rings can be obtained [56,76].

We tested the ability of HupA$_{6xHis}$ to stimulate cyclization of a [ɣ-$^{32}$P]-labelled 123-bp DNA fragment (Fig. 6A). The addition of T4 DNA-ligase alone results in multiple species, corresponding to ExoIII-sensitive linear multimers (Fig. 6A, lane 2 and 3). In the presence of HupA$_{6xHis}$, however, an ExoIII-resistant band is visible (Fig. 6A, lanes 4 to 6). In the absence of ExoIII, the linear dimer is still clearly visible in the HupA-containing samples (Fig. 6A, last lane). We conclude that *C. difficile* HupA is able to bend the DNA, or otherwise stimulate cyclization by increasing flexibility and reducing the distance between the DNA fragment extremities, allowing the ring closure in the presence of ligase.

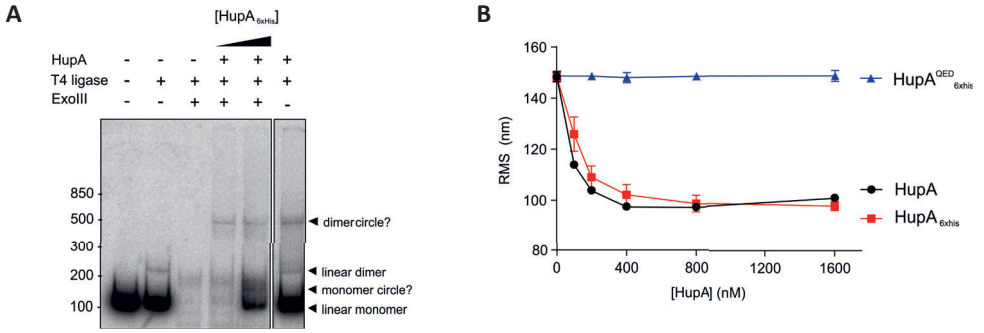


**Fig. 6 - HupA alters the topology of DNA in vitro. A)** Ligase-mediated cyclization assay. A 119-bp [ɣ-$^{32}$P]ATP-labelled dsDNA fragment was incubated in the presence of increasing concentrations of HupA$_{6xHis}$ (1, 10 µM), exonuclease III and ligase, as indicated above the panel. The presence of ExoIII-resistant (i.e., circular) DNA fragments is observed when samples are incubated with HupA$_{6xHis}$ ("circle").

**B)** The effect of increasing concentrations of HupA (black circles), $HupA_{6xHis}$ (red squares), and $HupA^{QED}_{6xHis}$ (blue triangles) on DNA conformation in TPM experiments. RMS (see Eq. (1)/ Materials and Methods) values as a function of protein concentration are shown. Increasing concentrations of HupA and $HupA_{6xHis}$ lead to a decreased RMS, suggesting compaction of the DNA.

To more directly demonstrate remodelling of DNA by HupA, we performed tethered particle motion (TPM) experiments. TPM is a single molecule technique that provides a readout of the length and flexibility of a DNA tether (Fig. S3) [77]. The binding of proteins to DNA alters its conformation, resulting in a change in RMS (Root Mean Square). If a protein bends DNA, makes DNA more flexible or more compact, the RMS is reduced compared to that of bare DNA, as represented in Supplemental Fig. S3 [77]. If a protein stiffens DNA, the RMS is expected to be larger than that of bare DNA [78].

We performed TPM experiments according to established methods [78] to determine the effects of HupA on DNA conformation at protein concentrations from 0 – 1600 nM (Fig. 6B). For this assay, a non-tagged HupA was purified from *C. difficile* cells overexpressing HupA and compared to $HupA_{6xHis}$ to assess potential subtle effects of the 6xhistidine-tag on the protein functionality. The experiments show that binding of both native HupA and $HupA_{6xHis}$ to DNA reduces the RMS (Fig. 6B). The RMS of bare DNA is 148 ± 1.9 nm. In the presence of HupA at different concentrations (100, 200, 400 nM) the RMS decreases (113 ± 0.1 nm; 103 ± 0.7 nm and 97 ± 1.5 nm respectively). Even at higher concentrations of HupA (800, 1600 nM) the RMS is 97-100 nm. $HupA^{QED}_{6xHis}$ did not affect RMS even at high protein concentrations (Fig. 6B). The strongly reduced RMS of DNA bound by non-tagged HupA at 1600 nM suggests a more compacted conformation of DNA compared to that of bare DNA. The curves are overall highly similar for HupA and $HupA_{6xHis}$ proteins; the small difference in the observed effects is attributed to interference of the tag and/or protein stability. The results obtained with the $HupA^{QED}_{6xhis}$ protein indicate that DNA binding by HupA is crucial for compaction, as expected.

The effects of *C. difficile* HupA of *C. difficile* on DNA topology observed by TPM indicates similar structural properties to those of *E. coli* HU, which was shown to compact DNA by bending at low protein coverage [26,79,80]. However, in contrast to *E. coli* [26], there is no clear stiffening of the DNA tether at high concentrations of protein in our assay, suggesting that there is lower or reduced dimer-dimer interaction in our experimental condition. Bending of DNA by HU proteins has also been shown for other organisms. Interestingly, in *B. burgdorferi* [55] and *Anabaena* [35] it was shown that bending is influenced by interaction of the DNA with a positively charged lateral surface, although the main interaction region with the DNA is through the β-arms. *C. difficile* HupA demonstrates an electrostatic surface potential

compatible with such a mechanism (Fig 1C). It will be of interest to determine if and which residues in this region contribute to the bending of the DNA.

**Overexpression of HupA decreases cell viability**

The condensation of the nucleoid and the slight increase of cell length during the timecourse of our microscopy experiments (Fig. 4B and C) could indicate that overexpression of HupA interferes with crucial cellular processes such as DNA replication. We, therefore, determined the long term effect of HupA overexpression on cell viability in a spot-assay (Fig. 7). In the absence of inducer, *C. difficile* strains harbouring inducible *hupA* genes grow as well as the vector control (AP34), with colonies visible at the $10^{-5}$ dilution. However, when induced with 200 ng/ml ATc viability is markedly reduced for strains overexpressing HupA (5-log; AP106), HupA-HaloTag (4-log; RD16) and HupA$^{QED}$-HaloTag (1 to 2-log; AF239) compared to the vector control. These effects are not due to a direct inhibitory effect of ATc alone, as the viability of AP34 is similar under both conditions.

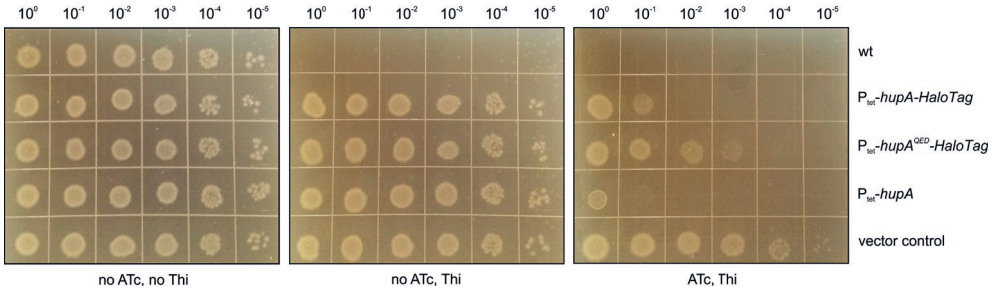


**Fig. 7 - Strain viability under conditions of HupA overexpression**. Spot assay of serially diluted *C. difficile* strains 630Δ*erm,* RD16 ($P_{tet}$-*hupA-HaloTag*), AF239 ($P_{tet}$-*hupA$^{QED}$-Halotag*), AP106 ($P_{tet}$-*hupA*) and AP34 ($P_{tet}$-*sluc$^{opt}$*). The left panel shows growth on medium with only *C. difficile* selective supplement (CDSS), the middle panel shows growth on medium with CDSS and thiamphenicol (Thi) and the right panel shows growth on medium with CDSS, Thi and 200 ng/mL anhydrotetracycline (ATc) after 24 hours at 37ºC. The results were verified by four independent spot assays and a typical image is shown. Overexpression of HupA strongly reduces cell viability.

We consistently observed a 1-log difference in cell viability between cells expressing HupA versus HupA-HaloTag (Fig. 7). This difference could be the result of slight interference of the HaloTag with HupA function, as also observed for the 6xhistagged protein in the TPM experiments (Fig. 6B). Considering that HupA$^{QED}$ does not appear to bind or compact DNA (Figs. 2, 5 and 6), the moderate reduction in cell viability compared to the vector control could be due to a dominant negative effect: the formation of heterodimers, consistent with our analysis (Fig. S2), could prevent a fraction of wild type HupA performing its essential function.

Overall, these results are consistent with a role of HupA in chromosome dynamics and underscore the importance of the nucleoid conformation on the cell survival.

## Conclusions

In this work, we present the first characterization of a bacterial chromatin protein in *C. difficile*. HupA is a member of the HU family of proteins and is capable of binding DNA and does so without an obvious difference in affinity as a result of the G+C content. DNA binding is dependent on the residues R55, R58 and R61 that are located in the predicted β-arm of the protein. These observations in combination with the predicted structure suggest a conserved mode of DNA binding, although the role of other regions of the protein in DNA binding is still poorly understood. HupA is present as a dimer in solution and disruption of the residues of the DNA binding domain did not affect the oligomeric state of HupA.

In *C. difficile* we co-localized HupA with the nucleoid and demonstrated that overexpression of HupA leads to nucleoid compaction and impairs *C. difficile* viability. In line with these observations, HupA stimulates the cyclization of a short dsDNA fragment and compacts DNA *in vitro*.

We also developed a new complementation assay for the detection of protein-protein interactions in *C. difficile,* complementing the available tools for this organism, and confirmed that HupA self-interacts *in vivo*. Additionally, to our knowledge, our study is the first to describe the use of the fluorescent tag HaloTag for imaging the subcellular localization of proteins in live *C. difficile* cells.

In sum, HupA of *C. difficile* is an essential bacterial chromatin protein required for nucleoid (re)modelling. HupA binding induces bending or increases the flexibility of the DNA, resulting in compaction. The function of HupA in chromosome dynamics *in vivo* remains to be determined. In *E. coli* conformational changes resulting from HU proteins enhance contacts between distant sequences in the chromosome [81]. In *Caulobacter*, HU proteins promote contacts between sequences in more close proximity [82]. These differences demonstrate that HU proteins may act differently *in vivo* despite high sequence similarity and that further research into the role of HupA in *C. difficile* physiology is needed.

## Methods

### Sequence Alignments and Structural Modelling

Multiple sequence alignment of amino acid sequences was performed with Clustal Omega [83]. The sequences of HU proteins identified in *C. difficile* 630Δ*erm* (Q180Z4), *E. coli* (P0ACF0 and P0ACF4), *Bacillus subtilis* (A3F3E2), *Geobacillus stearothermophilus* (P0A3H0), *Bacillus anthracis* (Q81WV7), *Staphylococcus aureus* (Q99U17), *Salmonella typhimurium* (P0A1R8), *Streptococcus pneumoniae* (AAK75224), *S. mutans* (Q9XB21), *M. tuberculosis* (P9WMK7), *Thermotoga maritima* (P36206) and *Anabaena sp.* (P05514), were selected for alignment. Amino acid sequences were retrieved from the Uniprot database.

Homology modelling was performed using PHYRE2 (http://www.sbg.bio.ic.ac.uk/phyre2, [51] and SWISS-MODEL [52] using default settings. For SWISS-MODEL, PDB 4QJN was used as a template. Selection of the template was based on PHYRE2 results, sequence identity (59,55%) and best QSQE (0,80) and GMQE (0,81). Graphical representations and mutation analysis were performed with the PyMOL Molecular Graphics System, Version 1.76.6. Schrödinger, LLC. For electrostatics calculations, APBS (Adaptive Poisson-Boltzmann Solver) and PDB2PQR software packages were used [84]. Default settings were used.

### Strains and growth conditions

*E. coli* strains were cultured in Luria Bertani broth (LB, Affymetrix) supplemented with chloramphenicol at 15 µg/mL or 50 µg/mL kanamycin when appropriate, grown aerobically at 37°C. Plasmids (Table 1) were maintained in *E. coli* strain DH5α. Plasmids were transformed using standard procedures [85]. *E. coli* strain Rosetta (DE3) (Novagen) was used for protein expression and *E. coli* CA434 for plasmid conjugation [86] with *C. difficile* strain 630Δ*erm* [64,87].

**Table 1 -** Plasmids used in this study.

| Name | Relevant features * | Source/Reference |
|---|---|---|
| pH6HTC | $P_{T7,}$ HaloTag-His6, *amp* | Promega |
| pCR2.1-TOPO | TA vector; pMB1 oriR; *km amp* | ThermoFisher |
| pET28b | $lacI^q$, $P_{T7}$ expression vector, *km* | Novagen |
| pRPF185 | *tetR* $P_{tet}$-*gusA*; *catP* | 63 |
| pAP24 | *tetR* $P_{tet}$-$sLuc^{opt}$; *catP* | 62 |
| pRD118 | $P_{T7}$-*sso685* | 88 |
| pAF226 | $P_{T7}$-$hupA_{6xHis}$; *km* | This study |
| pAF232 | $P_{T7}$-$hupA^{QE}{}_{6xHis}$; *km* | This study |
| pAF234 | $P_{T7}$-$hupA^{QED}{}_{6xHis}$; *km* | This study |
| pAF235 | *tetR* $P_{tet}$-$hupA^{QE}$-$HaloTag_{6xHis}$; *catP* | This study |
| pAF237 | *tetR* $P_{tet}$-$hupA^{QED}$-$HaloTag_{6xHis}$; *catP* | This study |
| pAF254 | *tetR* $P_{tet}$-$luc^{opt}$; *catP* | This study |
| pAF255 | *tetR* $P_{tet}$-*lgbit*; *catP* | This study |
| pAF256 | *tetR* $P_{tet}$-*hupA-smbit/lgbit*; *catP* | This study |
| pAF257 | *tetR* $P_{tet}$-*smBit/hupA-lgbit*; *catP* | This study |
| pAF259 | *tetR* $P_{tet}$-$bitluc^{opt}$; *catP* | This study |
| pAF260 | *tetR* $P_{tet}$-*smbit*; *catP* | This study |
| pAF262 | *tetR* $P_{tet}$-*smbit/lgbit*; *catP* | This study |
| pAP103 | *tetR* $P_{tet}$-*hupA*; *catP* | This study |
| pAP118 | *tetR* $P_{tet}$-*hupA-smbit/hupA-lgbit*; *catP* | This study |
| pAP134 | *tetR* $P_{tet}$-*hupA/lgbit*; *catP* | This study |
| pAP135 | *tetR* $P_{tet}$-*hupA-smbit*; *catP* | This study |
| pAP159 | *tetR* $P_{tet}$-*sbit/lgbit* (GTT); *catP* | This study |
| pAP210 | *tetR* $P_{tet}$-$hupA^{QED}$-*smbit/hupA-lgbit*; *catP* | This study |
| pRD4 | *tetR* $P_{tet}$-$hupA$-$HaloTag_{6xHis}$; *catP* | This study |
| pWKS1744 | pCR2.1-TOPO with *hupA; km amp* | This study |
| pWKS1746 | pCR2.1-TOPO with $HaloTag_{6xHis}$; *km amp* | This study |

** amp* – ampicillin resistance cassette, *catP* – chloramphenicol resistance cassette, *km* – kanamycin resistance cassette

*C. difficile* strains were cultured in Brain Heart Infusion broth (BHI, Oxoid), with 0,5 % w/v yeast extract (Sigma-Aldrich), supplemented with 15 µg/mL thiamphenicol and *Clostridioides difficile* Selective Supplement (CDSS; Oxoid) when necessary. *C. difficile* strains were grown anaerobically in a Don Whitley VA-1000 workstation or a Baker Ruskinn Concept 1000 workstation with an atmosphere of 10% $H_2$, 10% $CO_2$ and 80% $N_2$.

The growth was followed by optical density reading at 600 nm. All the *C. difficile* strains are described in Table 2.

**Table 2 -** *C. difficile* strains used in this study.

| Name | Relevant Genotype/Phenotype* | Source/Reference |
|---|---|---|
| AP6 | *C. difficile* 630Δerm; $Erm^S$ | 64,87 |
| WKS1588 | *630Δerm* pRPF185; $Thia^R$ | This study |
| RD16 | *630Δerm* pRD4; $Thia^R$ | This study |
| AF239 | *630Δerm* pAF237; $Thia^R$ | This study |
| AP34 | *630Δerm* pAP24; $Thia^R$ | 62 |
| AP106 | *630Δerm* pAP103; $Thia^R$ | This study |
| AP122 | *630Δerm* pAP118; $Thia^R$ | This study |
| AP152 | *630Δerm* pAP134; $Thia^R$ | This study |
| AP153 | *630Δerm* pAP135; $Thia^R$ | This study |
| AP181 | *630Δerm* pAF254; $Thia^R$ | This study |
| AP182 | *630Δerm* pAF259; $Thia^R$ | This study |
| AP183 | *630Δerm* pAF256; $Thia^R$ | This study |
| AP184 | *630Δerm* pAF257; $Thia^R$ | This study |
| AP199 | *630Δerm* pAF255; $Thia^R$ | This study |
| AP201 | *630Δerm* pAF260; $Thia^R$ | This study |
| AP202 | *630Δerm* pAF262; $Thia^R$ | This study |
| AP212 | *630Δerm* pAP210; $Thia^R$ | This study |

* $Erm^S$ – Erythromycin sensitive, $Thia^R$ – Thiamphenicol resistant

**Construction of the *E. coli* expression vectors**

All oligonucleotides and plasmids from this study are listed in Tables 1 and 3.

To construct an expression vector for $HupA_{6xHis}$, the *hupA* gene (CD3496 from *C. difficile* 630 GenBank accession no. NC_009089.1) was amplified by PCR from *C. difficile* 630Δ*erm* genomic DNA using primers oAF57 and oAF58 (Table 3). The product was inserted into the *Nco*I-*Xho*I digested pET28b vector (Table 1) placing it under control of the T7 promoter, yielding plasmid pAF226.

**Table 3 -** Oligonucleotides used in this study.

| Name | Sequence (5'>3') * |
|---|---|
| oAF57 | GTCGCCATGGATGAATAAAGCTGAATTAGTATCAAAG |
| oAF58 | GACGCTCGAGTCCATTTATTATATCCTTTAATCC |
| oAF61 | CGCCAGGCCAGGGCTGTCACTGTGCAGCTCGTGGACGC |
| oAF62 | GCGTCCACGAGCTGCACAGTGACAGCCCTGGCCTGGCG |
| oAF63 | CATCAGGCAAGAGTAGTCACTGTGTAGCTCGTGGATGC |
| oAF64 | GCATCCACGAGCTACACAGTGACTACTCTTGCCTGATG |
| oAF65 | CATTAAGTATGAGTATTCTATGTATAGATCATTGATGC |
| oAF66 | GCATCAATGATCTATACATAGAATACTCATACTTAATG |
| oAF73 | CATTTGAGACAAGAGAACAGGCTGCTGAACAAGGAAGAAATCCAAGAG |
| oAF74 | CTTGGATTTCTTCCTTGTTCAGCAGCCTGTTCTCTTGTCTCAAATGTTC |
| oAF75 | GGCTGCTGAACAAGGAGATAATCCAAGAGATCCAGAGC |
| oAF76 | CTGGATCTCTTGGATTATCTCCTTGTTCAGCAGCCTG |
| oAF81 | GCTAGAATTCGCCACTGGCAGCAGCCAC |
| oAF82 | CCTAGAATTCCTGTCCTTCTAGTGTAGCCG |
| oAP47 | TAGGATCCTTATCCATTTATTATATCCTTTAATCC |
| oAP48 | CT GAGCTCCTGCAGTAAAGGAGAAAATTTTGTTTTTACACTTGAAGATTTTGTGG |
| oAP49 | TAGGATCCCTATGCTAGAATACGTTCAC |
| oAP54 | CTGAGCTCCTGCAGTAAAGGAGAAAATTTTGTTTTTACACTTGAAGATTTTGTG |
| oAP55 | TAGGATCCCTATAGAATTTCTTCAAAAAGTCTATAACCTGTAACACTGTTTATAGTTAC |
| oAP58 | GGATCCTATAAGTTTTAATAAAACTTTAAATAG |
| oAP59 | AGCTCAGATCTGTTAACGCTACGATCAAGC |
| oAP60 | GCTTGATCGTAGCGTTAACAGATCTGAGC |
| oAP61 | CTCCTTTACTGCAGCGATCGAGCTATAG |
| oAP62 | GAAGAAATTCTATAGCTCGATCGCTGCAG |
| oAP63 | GTTTTATTAAAACTTATAGGATCCCTAACTGTTTATAG |
| oAP64 | GATCTGAGCTCCTGCAGTAAAGGAGAAAATTTTGTGAATAAAGC |
| oAP65 | CTTATAGGATCCAGCTATAGAATTTCTTC |
| oAP66 | GATCTGAGCTCCTGCAGTAAAGGAGAAAATTTTGTTACAGGTTATAGAC |
| oAP67 | GCTCGATCGCTGCAGTAAAGGAGAAAATTTTGTTTTTACACTTGAAGATTTTGTG |
| oAP96 | GCAGTAAAGGAGAAAATTTTGTGTTTACACTTGAAGATTTTG |
| oAP97 | CACAAAATCTTCAAGTGTAAACACAAAATTTTCTCCTTTAC |
| oAP98 | GCAGTAAAGGAGAAAATTTTGTGACAGGTTATAGACTTTTTG |
| oAP99 | CTTCAAAAAGTCTATAACCTGTCACAAAATTTTCTCCTTTAC |
| oAP110 | CCCCTCGAGATCCATTTATTATATCCTTTAATCC |
| oRD5 | CAGGATCTGGTTCAGGAAGTCTCGAGGGTTCCGAAATCGGTACTGG |
| Sso10a-2Nde | ATACATATGCAACTTGAACGGCGTAAAAGAGGAACAATGG |
| Sso10a-2Bam685 | GGTGGATCCTTTTCATCCCTTTAGTTCTTCCAG |
| oWKS-1511 | CTCGAGTCAGGATCTGGTTCAGGAAGTGGTTCCGAAATCGGTACTGGCTTTCC |
| oWKS-1512 | GGATCCTTAGTGGTGATGGTGATGATGACC |
| oWKS-1519 | GAGCTCAAATTTGAATTTTTTAGGGGGAAAATACCGTGAATAAAGCTGAATTAGTATCAAAG |
| oWKS-1520 | CTCGAGACTTCCTGAACCAGATCCTGATCCATTTATTATATCCTTTAATCCTTTTC |

* Restriction enzyme sites used underlined

To generate the HupA triple mutant ($HupA^{QED}_{6xHis}$) site-directed mutagenesis was used according to the QuikChange protocol (Stratagene). Initially, the arginine at position 55 and at position 58 were simultaneously substituted for glutamine (R55Q) and glutamic acid (R58E) respectively, using primers oAF73/oAF74 (Table 3), resulting in pAF232 (Table 1). The arginine at position 61 was subsequently substituted for aspartic acid (R61D) using primer pair oAF75/oAF76 (Table 3) and pAF232 as a template, yielding pAF234 (Table 1). All the constructs were confirmed by Sanger sequencing.

**Construction of the *C. difficile* expression vectors**

To overexpress non-tagged HupA the *hupA* gene was amplified by PCR from *C. difficile 630Δerm* genomic DNA using primers oWKS-1519 and oAP47 (Table 3) and cloned into *SacI-BamHI* digested pRPF185 vector [63], placing it under control of the ATc-inducible promoter $P_{tet}$, yielding vector pAP103 (Table 1).

For microscopy experiments, HaloTag tagged protein (Promega) was used. The *halotag* gene was amplified from vector pH6HTC (Promega, GenBank Accession no. JN874647) with primers oWKS-1511/oWKS-1512 and inserted into pCR2.1-TOPO according to the instructions of the manufacturer (ThermoFisher), yielding vector pWKS1746 (Table 1). This primer combination also introduces a 6xHis-tag at the C-terminus of the HaloTag. The *hupA* gene was amplified with primers oWKS-1519/oWKS-1520 (Table 3) and inserted into vector pCR2.1-TOPO according to the instructions of the manufacturer (ThermoFisher), generating vector pWKS1744 (Table 1). The primers introduce the *cwp2* ribosomal binding site upstream and a short DNA sequence encoding a GS-linker downstream (SGSGSGS) of the *hupA* open reading frame. To generate the expression construct for HupA-Halotag the open reading frame encoding the $HaloTag_{6xHis}$ protein was amplified from pWKS1746 using primers oRD5/oWKS-1512 (Table 3). The *hupA* gene was amplified from pWKS1744 with primers oWKS-1519/oWKS-1520 (Table 3). Gene fusions were made by overlapping PCR using the PCR amplified fragments encoding HupA and Halotag proteins as templates with primers oWKS-1519 and oWKS-1512 (Table 3). The fragment was cloned into *SacI-BamHI* digested pRPF185 [63], placing it under control of the ATc inducible promoter $P_{tet}$, yielding vector pRD4 (Table 1).

To generate the HupA triple mutant fused to the Halotag ($HupA^{QED}$-Halotag) site-directed mutagenesis was used, according to the QuikChange protocol (Stratagene). The arginines at position 55 and at position 58 were substituted to glutamine (R55Q) and glutamic acid (R58E), using primers oAF73/oAF74 (Table 3) and pRD4 as template, resulting in pAF235 (Table 1). The arginine at position 61 was subsequently substituted to aspartic acid (R61D), using

pAF235 as template and primers oAF75/oAF76 (Table 3), yielding pAF237 (Table 1). All the constructs were confirmed by Sanger sequencing.

**Construction of the bitLuc$^{opt}$ expression vectors**

The bitLuc$^{opt}$ complementation assay for *C. difficile* described in this study is based on NanoBiT (Promega) [61] and the codon-optimized sequence of sLuc$^{opt}$ [62]. Details of its construction can be found in Supplemental Material.

Gene synthesis was performed by Integrated DNA Technologies, Inc. (IDT). Fragments were amplified by PCR from synthesized dsDNA, assembled by Gibson assembly [89] and cloned into *Sac*I/*BamH*I digested pRPF185 [63], placing them under control of the ATc-inducible promoter $P_{tet}$. As controls, a non-secreted luciferase (Luc$^{opt}$; pAF254) and a luciferase with the NanoBiT aminoacid substitutions (Promega) [61] (bitLuc$^{opt}$; pAF259) were constructed. We also constructed vectors expressing only the SmBiT and LgBiT domains, alone (pAF260 and pAF255) or in combination (pAF262), as controls.

To assay for a possible interaction between HupA monomers, vectors were constructed that encode HupA-SmBiT/HupA-LgBiT (pAP118), HupA$^{QED}$-SmBiT/HupA-LgBiT (pAP210), HupA-SmBiT/LgBiT (pAF256), SmBiT/HupA-LgBiT (pAF257). DNA sequences of the cloned DNA fragments in all recombinant plasmids were verified by Sanger sequencing.

Note that all our constructs use the HupA start codon (GTG) rather than ATG; a minimal set of vectors necessary to perform the *C. difficile* complementation assay (pAP118, pAF256, pAF257 and pAF258) is available from Addgene (105494-105497) for the *C. difficile* research community.

**Overproduction and purification of HupA$^{QED}_{6xhis}$ and HupA-HaloTag**

Overexpression of HupA$_{6xHis}$ and HupA$^{QED}_{6xHis}$ was carried out in *E. coli* Rosetta (DE3) strains (Novagen) harbouring the *E. coli* expression plasmids pAF226 and pAF234, respectively. Cells were grown in LB and induced with 1mM isopropyl-β-D-1-thiogalactopyranoside (IPTG) at an optical density ($OD_{600}$) of 0.6 for 3 hours. The cells were collected by centrifugation at 4°C and stored at -80°C.

Overexpression of HupA-HaloTag (which also includes a 6xhistag) was carried out in *C. difficile* strains RD16. Cells were grown until $OD_{600}$ 0.4-0.5 and induced with 200 ng/mL ATc for 1 hour. Cells were collected by centrifugation at 4°C and stored at -80°C.

Pellets were suspended in lysis buffer (50 mM $NaH_2PO_4$ (pH 8.0), 300 mM NaCl, 10 mM imidazole, 5 mM β mercaptoethanol, 0.1% NP40 and Complete protease inhibitor cocktail (CPIC, Roche Applied Science). Cells were lysed by the addition of 1 mg/ml lysozyme and sonication. The crude lysate was clarified by centrifugation at 13000 g at 4°C for 20 min. The supernatant containing recombinant proteins was collected and purification was performed with TALON Superflow resin (GE Healthcare) according to the manufacturer's instructions. Proteins were stored at -80°C in 50 mM $NaH_2PO_4$ (pH 8.0), 300 mM NaCl and 12% glycerol.

**Overproduction and purification of non-tagged HupA**

Overexpression of HupA was carried out in *C. difficile* strain AP106 that carries the plasmid encoding HupA under the ATc-inducible promoter $P_{tet}$. Cells were grown until $OD_{600}$ 0.4-0.5 and induced with 200 ng/mL ATc for 3 hours. Cells were collected by centrifugation at 4°C.

Pellets were resuspended in HB buffer (25 mM Tris (pH 8.0), 0.1 mM EDTA, 5 mM β mercaptoethanol, 10% glycerol and CPIC). Cells were lysed by French Press and phenylmethylsulfonyl fluoride was added to 0.1 mM. Separation of the soluble fraction was performed by centrifugation at 13000g at 4°C for 20 min. Purification of the protein from the soluble fraction was done on a 1 mL HiTrap SP (GE Healthcare) according to manufacturer instructions. The protein was collected in HB buffer supplemented with 300 mM NaCl. Fractions containing the HupA protein were pooled together and applied to a 1 mL Heparin Column (GE Healthcare) according to the manufacturer's instructions. Column washes were performed with a 500 mM – 800 mM NaCl gradient in HB buffer. Proteins were eluted in HB buffer supplemented with 1 M NaCl and stored in 10% glycerol at -80°C.

**DNA labelling and electrophoretic mobility shift Assay (EMSA)**

For the gel shift-assays, double-stranded oligonucleotides with different [G+C] contents were used. Oligonucleotides oAF61/oAF62 have a 71.1% [G+C]-content, oAF63/oAF64 have a 52.6% G+C-content and oAF65/oAF66 have a 28.9% [G+C]-content. The oligonucleotides were labelled with [ɣ-$^{32}$P]ATP and T4 polynucleotide kinase (PNK) (Invitrogen) according to the PNK-manufacturer's instructions. The fragments were purified with a Biospin P-30 Tris column (BioRad). Oligonucleotides with same [G+C] content were annealed by incubating them at 95˚C for 10 min, followed by ramping to room temperature.

Gel shift assays were performed with increasing concentrations (0.25 -2 µM) of $HupA_{6xHis}$ or $HupA^{QED}_{6xHis}$ in a buffer containing 20 mM Tris pH 8.0; 50 mM NaCl; 12 mM $MgCl_2$; 2.5 mM ATP; 2 mM DTT; 10% glycerol and 2.4 nM [ɣ-$^{32}$P]ATP-labelled oligonucleotides. Proteins were

incubated with the oligonucleotide substrate for 20 min at room temperature prior to separation. Reactions were analyzed in 8% native polyacrylamide gels in cold 0,5X TBE buffer supplemented with 10 mM $MgCl_2$. After electrophoresis gels were dried under vacuum and protein-DNA complexes were visualized by phosphorimaging (Typhoon 9410 scanner; GE Healthcare). Analysis was performed with Quantity-One software (BioRad).

**Size-exclusion chromatography**

Size-exclusion experiments were performed on an Äkta pure 25L1 instrument (GE Healthcare). 200 µL of $HupA_{6xHis}$ and $HupA^{QED}{}_{6xHis}$ was applied at a concentration of ~100 µM, to a Superdex 75 HR 10/30 column (GE Healthcare), in buffer containing 50 mM $NaH_2PO_4$ (pH 8.0), 300 mM NaCl and 12% glycerol. UV detection was done at 280 nm. Lower concentrations of HupA were not possible to analyses due to the lack of signal. HupA protein only contains 3 aromatic residues and lacks His, Trp, Tyr or Cys to allow detection by absorbance at 280 nm. The column was calibrated with a mixture of proteins of known molecular weights (Mw): conalbumin (75 kDa), ovalbumin (44 kDa), carbonic anhydrase (29 kDa), ribonuclease A (13,7 kDa), and aprotinin (6,5 kDa). Molecular weight of the HupA proteins was estimated according to the equation MW=10(Kav-b)/m where m and b correspond to the slope and the linear coefficient of the plot of the logarithm of the MW as a function of the Kav. The Kav is given by the equation $Kav=(V_e-V_0)/(V_t-V_0)$ [90], where $V_e$ is the elution volume for a given concentration of protein, $V_0$ is the void volume (corresponding to the elution volume of thyroglobulin), and $V_t$ is the total column volume (estimated from the elution volume of a 4% acetone solution).

**Glutaraldehyde cross-linking Assay**

100 ng HupA protein was incubated with different concentrations of glutaraldehyde (0 0,006%) for 30 min at room temperature. Reactions were quenched with 10 mM Tris. The samples were loaded on a 6.5% SDS-PAGE gel and analysed by western blotting. The membrane was probed with a mouse anti-His antibody (Thermo Fisher) 1:3000 in phosphate buffered saline (PBS; 137 mM NaCl, 2.7 mM KCl, 4.3 mM $Na_2HPO_4$, 1.47 mM $KH_2PO_4$) with 0.05% Tween-20 and 5% w/v Milk (Campina), a secondary anti-mouse HRP antibody 1:3000 and Pierce ECL2 Western blotting substrate (Thermo Scientific). A Typhoon 9410 scanner (GE Healthcare) was used to record the chemiluminescent signal.

**Split luciferase ($bitLuc^{opt}$) Assay**

For the *C. difficile* complementation assay, cells were grown until $OD_{600}$ 0.3-0.4 and induced with 200 ng/mL anhydrotetracycline for 60 min. To measure luciferase activity 20 µL NanoGlo

Luciferase (Promega N1110) was added to 100 µL of culture sample. Measurements were performed in triplicate in a 96-well white F-bottom plate according to manufacturer's instructions. Luciferase activity was determined using a GloMax instrument (Promega) for 0.1 s. Data was normalized to culture optical density measured at 600 nm ($OD_{600}$). Statistical analysis was performed with Prism 7 (GraphPad, Inc, La Jolla, CA) by two-way ANOVA.

**Ligase-mediated cyclization assay**

A 119 bp DNA fragment was amplified by PCR amplification with primers oAF81/oAF82, using pRPF185 plasmid as a template. The PCR fragment was digested with *EcoR*I and 5'end labelled with [$\gamma^{32}$P] ATP using T4 polynucleotide kinase (Invitrogen) according to the manufacturer's instructions. Free ATP was removed with a Biospin P-30 Tris column (BioRad).

The labelled DNA fragment (~0.5 nM) waspAF235 incubated with different concentrations of HupA for 30 min on 30°C in 50 mM Tris-HCl, pH 7.8, 10 mM $MgCl_2$, 10 mM DTT, and 0.5 mM ATP in a total volume of 10 µl. 1 Unit of T4 ligase was added and incubated for 1 h at 30°C followed by inactivation for 15 minutes at 65°C. When appropriate, samples were treated with 100 U of Exonuclease III (Promega) at 37°C for 30 minutes. Enzyme inactivation was performed by incubating the samples for 15 minutes at 65°C. Before electrophoresis, the samples were digested with 2 µg proteinase K and 0.2% SDS at 37°C for 30 minutes. Samples were applied to a pre-run 7% polyacrylamide gel in 0.5X TBE buffer with 2% glycerol and run at 100V for 85 min. After electrophoresis, the gel was vacuum-dried and analysed by phosphorimaging. Analysis was performed with Quantity-One software (BioRad).

**Fluorescence microscopy**

The sample preparation for fluorescence microscopy was carried out under anaerobic conditions. *C. difficile* strains were cultured in BHI/YE, and when appropriate induced with different ATc concentrations (50, 100 and 200 ng/mL) for 1 hour at an $OD_{600}$ of 0.3-0.4. When required, cells were incubated with 150 nM Oregon Green substrate for HaloTag (Promega) for 30 min. 1 mL culture was collected and washed with pre-reduced PBS. Cells were incubated with 1 µM DAPI (Roth) when necessary. Cells were spotted on 1.5% agarose patches with 1 µL of ProLong Gold antifading mountant (Invitrogen). Slides were sealed with nail polish.

Samples were imaged with a Leica DM6000 DM6B fluorescence microscope (Leica) equipped with DFC9000 GT sCMOS camera using a HC PLAN APO 100x/1.4 OIL PH3 objective, using the LAS X software. The filter set for imaging DAPI is the DAPI ET filter (n. 11504203, Leica), with excitation filter 350/50 (bandpass), long pass dichroic mirror 400 and emission filter 460/50

(bandpass). For imaging of Oregon Green the filter L5 ET was used (n. 11504166, Leica), with excitation filter 480/40, dichroic mirror 505 and emission filter 527/30.

Data was analyzed with MicrobeJ package version 5.12d [91] with ImageJ 1.52d software [92]. Recognition of cells was limited to 2 - 16 µm length. For the nucleoid and Halotag detection the nucleoid feature was used for the nucleoid length and fluorescent analysis. Cells with more than 2 identified nucleoids and defective detection were excluded from analysis. Statistical analysis was performed with MicrobeJ package version 5.12d [91].

**In-gel fluorescence**

*C. difficile* strains were cultured in BHI/YE, and when appropriate induced at an $OD_{600}$ of 0.3-0.4 with 200 ng/mL ATc concentrations for up to 3 hours. Samples were collected and centrifuged at 4°C. Pellets were resuspended in PBS and lysed by French Press. Samples were incubated with 150 nM Oregon Green substrate for HaloTag (Promega) for 30 minutes at 37°C. Loading buffer (250 mM Tris-Cl pH 6.8, 10 % SDS, 10% β-mercaptoethanol, 50% glycerol, 0.1% bromophenol blue) was added to the samples without boiling and samples were run on 12% SDS-PAGE gels. Gels were imaged with Uvitec Alliance Q9 Advanced machine (Uvitec) with F-535 filter (460 nm).

**Spot-assay**

Cells were grown until $OD_{600}$ of 1.0 in BHI/YE and pre-induced with 200 ng/mL ATc for 3 hours. Cells were collected by centrifugation at 4°C. The cultures were serially diluted ($10^0$ to $10^{-5}$) and 2 µL from each dilution were spotted on BHI/YE supplemented with CDSS, thiamphenicol and 200 ng/mL ATc when appropriate. Plates were imaged after 24 hours incubation at 37ºC.

**Tethered Particle Motion measurements**

A dsDNA fragment of 685bp with 32% [G+C] content (sso685) was used for Tethered Particle Motion experiments. This substrate was generated by PCR using the forward biotin-labelled primer Sso10a-2Nde and the reverse digoxygenin (DIG) labelled primer Sso10a-2Bam685 from pRD118 as previously described [88]. The PCR product was purified using the GenElute PCR Clean-up kit (Sigma-Aldrich).

Tethered Particle Motion (TPM) measurements were done as described previously [77,78] with minor modifications. In short, anti-digoxygenin (20 µg/mL) was flushed into the flow cell and incubated for 10 minutes to allow the anti-digoxygenin to attach to the glass surface. To block unspecific binding to the glass surface, the flow cell was incubated with BSA and BGB (Blotting

grade Blocker) in buffer A (10 mM Tris (pH 7.5), 150 mM NaCl, 1 mM EDTA, 1 mM DTT, 3% glycerol, and 100 µg/mL acetylated BSA, 0.4% BGB) for 10 minutes. To tether DNA to the surface, DNA (labelled with Biotin and DIG) diluted in buffer B (10 mM Tris (pH 7.5), 150 mM NaCl, 1 mM EDTA, 1 mM DTT, 3% glycerol, and 100 µg/mL acetylated BSA) was flushed into the flow cell and incubated for 10 minutes. Streptavidin-coated polystyrene beads (0.44 µm in diameter) diluted in buffer B were introduced into the sample chamber and incubated for at least 10 minutes to allow binding to the biotin-labelled DNA ends. Before flushing in the protein in buffer C (20 mM HEPES (pH 7.9), 60 mM KCl, and 0.2% (w/v) BGB), the flow cell was washed twice with buffer C to remove free beads. Finally, the flow cell was sealed, followed by incubation with protein or experimental buffer for 10 minutes. The measurements were started after 6 minutes of further incubation of the flow cell at a constant temperature of 25 °C. More than 300 beads were measured for each individual experiment. All experiments were performed at least in duplicate.

The analysis of the TPM data was performed as previously described [78]. Equation 1 was used to calculate the RMS of the individual beads.

$$RMS = \sqrt{\frac{1}{n}\sum_{i=1}^{n}[(x_i - \overline{x})^2 + (y_i - \overline{y})^2]} \qquad \text{Equation 1}$$

where x and y are the coordinates of the beads, $\overline{x}$ and $\overline{y}$ are averaged over the full-time trace. The RMS value of each measured condition was acquired by fitting a Gaussian to the histogram of the RMS values of individual beads.

All the pictures were prepared for publication in CorelDRAW X8 (Corel).

## Acknowledgements

Work in the group of WKS is supported by a Vidi Fellowship (864.10.003) of the Netherlands Organization for Scientific Research (NWO) and a Gisela Their Fellowship from the Leiden University Medical Center. Work in the group of RTD is supported by a VICI grant (016.160.613) of the Netherlands Organization for Scientific Research (NWO), Human Frontier Science Program [RGP0014/2014] and a China Scholarship Council to L.Q. [201506880001]. The authors thank Jeroen Corver for helpful discussions and Patricia Amaral for her assistance with the graphical abstract.

## Conflict of interest

WKS has performed research for Cubist. The company had no role in the design or interpretation of these experiments or the decision to publish. Others: none to declare.

## Supplemental Figures

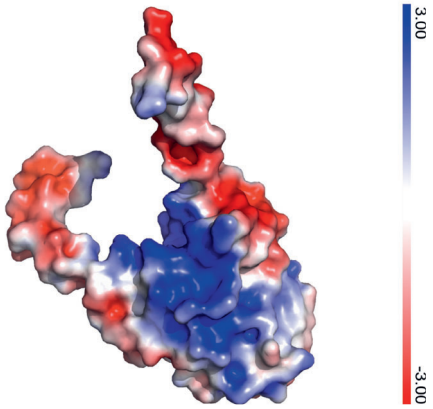


**Fig. S1 - Electrostatic surface potential of *C. difficile* HupA$^{QED}$**. The electrostatic potential is in eV with the range shown in the corresponding color bar.

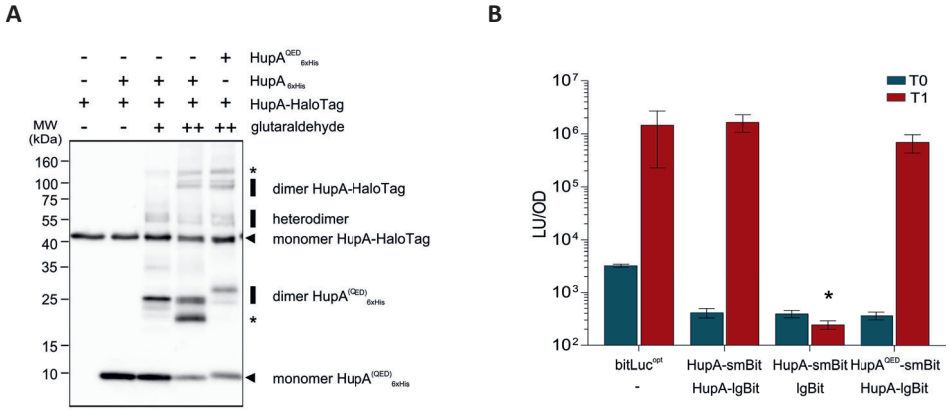


**Fig. S2 - – HupA$^{QED}$ can interact with HupA. A)** Western-blot analysis of glutaraldehyde cross-linking of HupA-HaloTag with HupA$_{6xhis}$ and HupA$^{QED}_{6xhis}$. 100 ng of the indicated proteins were incubated with 0%, 0.0006% and 0.006% glutaraldehyde for 30 min at room temperature. The samples were resolved by SDS-PAGE and analysed by immunoblotting with anti-his antibody. Crosslinking between HupA-HaloTag (46 kDa) and the HupA$^{(QED)}_{6xHis}$ monomers (11 kDa) resulted in bands corresponding to the approximate molecular weight of homodimers of HupA$^{(QED)}_{6xHis}$ (22 kDa), homodimers of HupA-HaloTag (92 kDa) and heterodimers (57 kDa). Additional bands of lower molecular weight HupA are observed that likely represent breakdown products and an unknown species is observed higher in the gel (both indicated with *). No difference is evident between the crosslinking with HupA$_{6xhis}$ and HupA$^{QED}_{6xhis}$, suggesting both can form mixed multimers with HupA-HaloTag. **B)** Luciferase activity of strains AP182 (P$_{tet}$-*bitluc$^{opt}$*), AP122 (P$_{tet}$-*hupA-smbit/hupA-lgbit*), AP184 (P$_{tet}$-*smbit-hupA/lgbit*) and AP212 (P$_{tet}$-*hupA$^{QED}$-smbit/hupA-*

*lgbit*). Cells were induced with 200 ng/mL anhydrotetracycline (ATc) for 60 min. Optical density-normalized luciferase activity (LU/OD) is shown right before induction (T0, blue bars) and after 1 hour of induction (T1, red bars). The averages of biological duplicate measurements are shown, with error bars indicating the standard deviation from the mean. A positive interaction was defined on the basis of the negative control (AP184) as a luciferase activity of >1000 LU/OD. No significant difference was detected at T0. At T1, only AP184 was significantly different from all other samples with *p<0.0001 by two-way ANOVA.

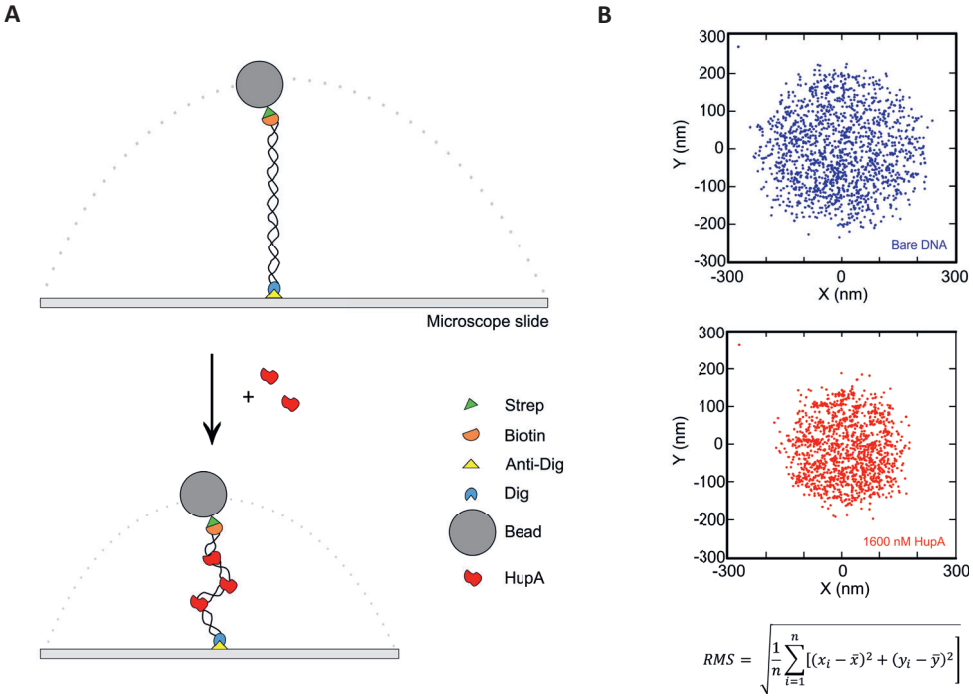


**Fig. S3 - Schematic representation of tethered particle motion experiments. A)** The dsDNA molecule is labelled with digoxygenin (Dig, yellow) and biotin (orange). The dsDNA is tethered via the anti-digoxigenin antibody (anti-Dig, blue) linked to the microscope slide surface and via the streptavidin (Strep, green) linked to the bead (grey). The dotted line represents the amplitude of the bead movement. Addition of HupA leads to DNA compaction, evident as a restriction of bead movement. **B)** Excursion of the bead with bare DNA (blue) and with 1600 nM HupA (red) on x-y coordinates. The root mean square (RMS) value of the excursion of each individual bead was calculated from the x- and y-coordinates, as represented by the equation.

## Supplemental Methods

### Construction of a split-luciferase system for *C. difficile*

We stepwise adapted our sLuc$^{opt}$ reporter [62] by 1) removing the signal sequence (resulting in an intracellular luciferase, Luc$^{opt}$), 2) introducing the mutations corresponding to the aminoacid substitutions in NanoBiT (resulting in a full-length luciferase in which SmBiT and LgBiT are fused, bitLuc$^{opt}$) and finally, 3) the construction of a modular vector containing polycistronic construct under the control of the ATc-inducible promoter $P_{tet}$ [63,93].

Modules for the vectors to be constructed were synthesized dsDNA fragments based on the codon-optimized sLuc$^{opt}$ sequence, but carrying the desired point mutations. Gene synthesis was performed by Integrated DNA Technologies, Inc. All primers and plasmids are listed in Tables 1 and 3. DNA sequences of the cloned DNA fragments in all recombinant plasmids were verified by sequencing.

The *hupA-smbit* and *hupA-lgbit* fragments with restriction sites to ensure modularity of the vectors were amplified with primers oAP60/oAP65 and oAP63/oAP64, respectively, cut with *Sac*I-*Bam*HI and cloned into similarly digested pRPF185, yielding plasmid pAP135 ($P_{tet}$-*hupA-smbit*) and pAP134 ($P_{tet}$-*hupA-lgbit*). To construct the plasmid harbouring an operon encoding HupA-SmBiT and HupA-LgBiT Gibson assembly was performed. The pRPF185 plasmid backbone was PCR amplified with primer set oAP58/oAP59. The *hupA-smBit* fragment was amplified from pAP135 using primers oAP60/oAP61, and the *hupA-lgBit* fragment was amplified from pAP134 using primers oAP62/oAP63. All the PCR fragments were purified and assembled at 50°C for 30 min in Gibson assembly mix [5% PEG-8000, 10 mM $MgCl_2$, 100 mM Tris-HCl pH 7.5, 10 mM DTT, 0.8 mM dNTPs, 5 mM NAD, 5.33 U/µL Taq Ligase (Qiagen), 0.005 U/µL T5 exonuclease (NEB), 0.03 U/µL Phusion polymerase (NEB)], yielding pAP118 ($P_{tet}$-*hupA-smbit*/*hupA-lgbit*). The resulting operon contains the same ribosome binding site in front of both open reading frames.

To introduce the QED mutation in pAP118, the gene encoding for *hupA$^{QED}$* was amplified from pAF237 with primer set oAP64/oAP110. The fragment was digested with *SacI*/*XhoI* and ligated into the similarly digested pAP118, yielding pAP210.

As controls for HupA-dependency of a possible interaction, HupA-fusions were expressed from the same operon as individual luciferase domains (either SmBiT or LgBiT). To construct $P_{tet}$-*hupA-smbit/lgbit,* pAP159 was *BamH*I/*Pvu*I digested, the 511 bp fragment was gel purified, and ligated into the similarly digested pAP118 vector. As the *lgbit* lacked a characterized start codon (GTT), the first triplet was replaced with GTG (as in HupA) according

to the QuikChange protocol (Stratagene) with primer set oAP98/oAP99, yielding vector pAF256.

To construct $P_{tet}$-*smbit/hupA-lgBit*, pAP118 was *BamH*I/*Pvu*I digested, the 838 bp fragment was gel purified and ligated into similarly digested pAP159. As the *smbit* lacked a characterized start codon (GTT), the first triplet was replaced with GTG (as in HupA) according to the QuikChange protocol (Stratagene) with primer set oAP96/oAP97, yielding vector pAF257.

As positive controls, *C. difficile* expression plasmids encoding non-secreted luciferase ($Luc^{opt}$) and luciferase with the aminoacid substitutions ($bitLuc^{opt}$) (Promega) [61] were constructed. $Luc^{opt}$ was amplified from pAP24 [62] with primers oAP48/oAP49, digested with *BamH*I/*Sac*I and cloned into similarly digested pRPF185. As the other controls, the start codon was replaced with GTG according to the QuikChange protocol (Stratagene) with primer set oAP98/oAP99, yielding plasmid pAF254.

To construct $bitLuc^{opt}$, the *lgbit* gene was amplified from pAP134 with primers oAP54/oAP55 (Table 3) digested with *BamH*I/*Sac*I and cloned into similarly digested pRPF185. The start codon was replaced with GTG according to the QuikChange protocol (Stratagene) with primer set oAP98/oAP99, yielding plasmid pAF259.

Vectors encoding just SmBiT and LgBiT (not part of a fusion protein) were constructed as negative controls. The *lgbit* gene was amplified from pAP134 using primer oAP54/oAP63 and the fragment digested with *BamH*I/*Sac*I, and cloned into similarly digested pRPF185. The start codon was replaced with GTG according to the QuikChange protocol (Stratagene) with primer set oAP98/oAP99, yielding plasmid pAF255. The *smbit* gene was amplified from pAP135 using primer oAP66/oAP65. The fragments were *BamH*I and *Sac*I digested, and cloned into similarly digested pRPF185. As described above, the start codon was changed to GTG with primers oAP97/oAP96, yielding pAF260.

To construct the negative control plasmid harbouring both *smbit* and *lgbit* as part of the same operon, *smbit* and *lgbit* DNA fragments were generated by PCR from pAP135 using primers oAP66/oAP61 and from pAP134 using oAP67/oAP63, respectively. The fragments were fused by overlapping PCR with primers oAP66/oAP63, digested with *BamH*I/*Sac*I and cloned into similarly digested pRPF185. As described above, the start codon was changed to GTG with primers set oAP98/oAP99 and oAP97/oAP96, yielding pAF262.

It should be noted that due to the use of the GTG start codon (similar to HupA) and the fact that fusions with the luciferase domains are C-terminal, it may be necessary to adapt the start codons of the control plasmids to that of other proteins of interest when using this system.

Schematic representations of the modular vectors constructed for this study is shown in Figure SM1.

We previously described the codon optimization of the NanoLuc luciferase as part of the construction of a secreted luciferase reporter, sLuc$^{opt}$, for *C. difficile* [62]. The *C. difficile* complementation assay requires proteins to remain intracellular. Therefore, we first constructed a non-secreted luciferase reporter by removing the PPEP-1 signal sequence from sLuc$^{opt}$, yielding Luc$^{opt}$.

For the complementation assay the substitution of specific residues was necessary to reduce spontaneous interactions between the small and large subunits of the split luciferase were necessary [61]. To determine if these substitutions potentially reduce the maximum levels of luminescence of the reconstituted luciferase, we introduced them in Luc$^{opt}$, yielding bitLuc$^{opt}$ (Luc$^{opt}$-R11E/G15A/F31L/G35A/L46R/G51A/G67A/G71A/K75E/ I76V/H93P/I107L/D108N/N144T/L149M/G157S/W161Y/C164F/R166E), and assayed luminescence in the presence and absence of anhydrotetracycline. No significant difference between Luc$^{opt}$ and bitLuc$^{opt}$ was observed (Fig. SM2B), indicating that the substitutions in bitLuc$^{opt}$ did not alter luciferase expression and activity.

Finally, we wanted to establish whether the expression of the individual subunits of the split luciferase, alone or in combination, without fusion protein would result in a positive signal in the luciferase assay. The bitLuc$^{opt}$ luciferase was split into the two subunits: lgBit (19 kDa) and smBit (1.3 kDa). When the two subunits are expressed individually or from the same operon no significant difference was observed in the luciferase signal after induction (Fig. SM2B). This demonstrates that there is no non-specific binding of the bitLuc$^{opt}$ sub-units in *C. difficile* that could interfere with its application as a complementation assay.

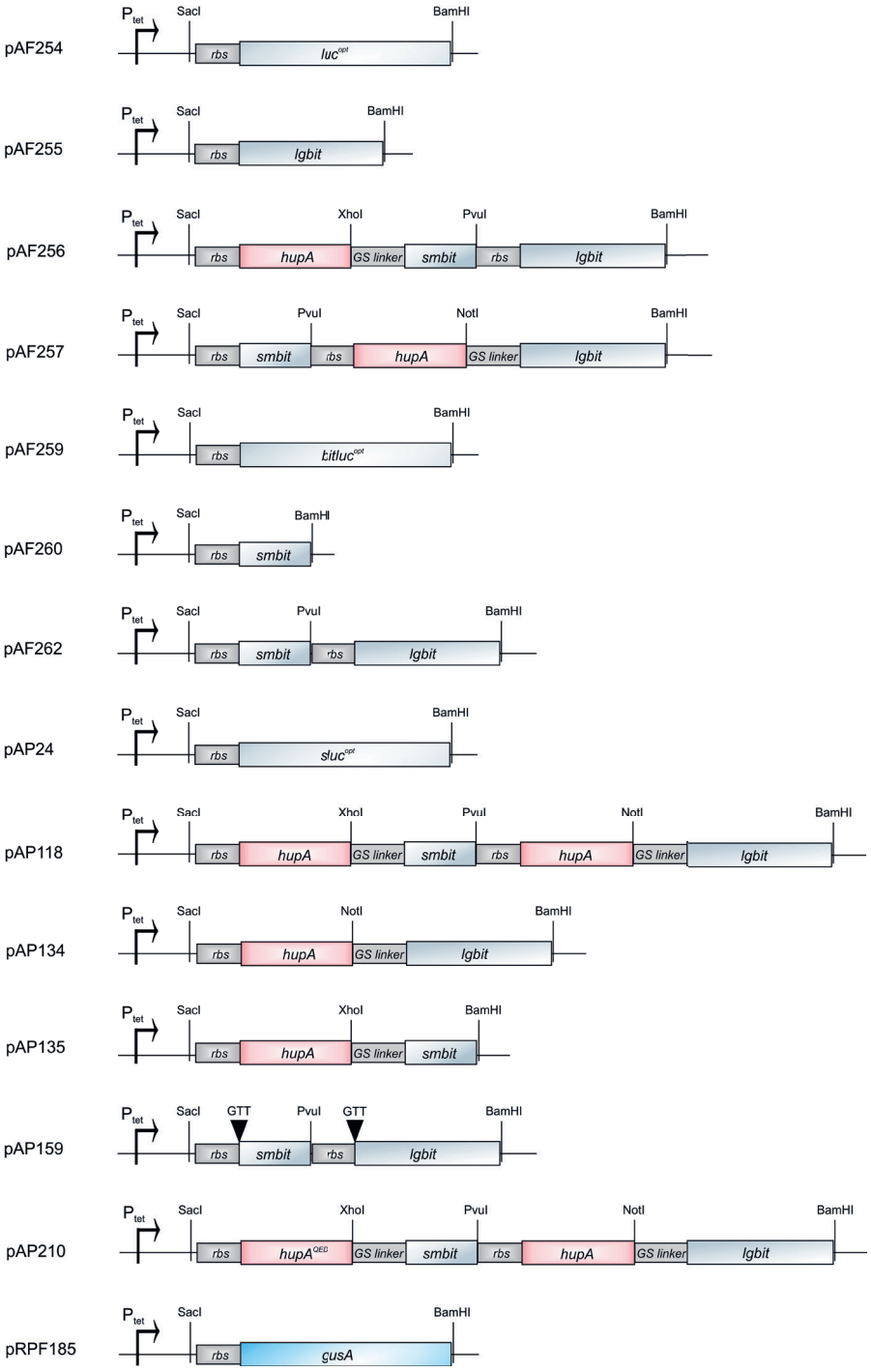
pAF254
P tet
SacI
BamHI
rbs
luc opt
pAF255
P tet
SacI
BamHI
rbs
lgbit
pAF256
P tet
SacI
XhoI
PvuI
BamHI
rbs
hupA
GS linker
smbit
rbs
lgbit
pAF257
P tet
SacI
PvuI
NotI
BamHI
rbs
smbit
rbs
hupA
GS linker
lgbit
pAF259
P tet
SacI
BamHI
rbs
bitluc opt
pAF260
P tet
SacI
BamHI
rbs
smbit
pAF262
P tet
SacI
PvuI
BamHI
rbs
smbit
rbs
lgbit
pAP24
P tet
SacI
BamHI
rbs
sluc opt
pAP118
P tet
SacI
XhoI
PvuI
NotI
BamHI
rbs
hupA
GS linker
smbit
rbs
hupA
GS linker
lgbit
pAP134
P tet
SacI
NotI
BamHI
rbs
hupA
GS linker
lgbit
pAP135
P tet
SacI
XhoI
BamHI
rbs
hupA
GS linker
smbit
pAP159
P tet
SacI
GTT
PvuI
GTT
BamHI
rbs
smbit
rbs
lgbit
pAP210
P tet
SacI
XhoI
PvuI
NotI
BamHI
rbs
hupA QED
GS linker
smbit
rbs
hupA
GS linker
lgbit
pRPF185
P tet
SacI
BamHI
rbs
gusA

**Fig. SM1 - Schematic representation of the modular vectors of the bitLuc$^{opt}$ complementation assay.** When expressing sLuc$^{opt}$ and Luc$^{opt}$ in *C. difficile* we detected in a significant increase of luciferase signal of the culture 1 hour after induction (Fig. SM2A). At the moment of induction Luc$^{opt}$ exhibit a luciferase signal of, slightly over the background signal of medium itself (235 ± 245 LU). After induction, a significant increase in luminescence is observed for both sLuc$^{opt}$ and Luc$^{opt}$. sLuc$^{opt}$ induction results in a signal of 2.9e$^{+8}$ ± 4.5e$^{+7}$ LU/OD, whereas significantly lower signals were detected with Luc$^{opt}$ induction (2472785 ± 910696 LU/OD). However, the signal from a non-induced Luc$^{opt}$ (4801 ± 946 LU/OD) is lower than for the non-induced sLuc$^{opt}$ (535140 ± 44572 LU/OD), resulting in similar ~3 log increase in signal upon induction for both reporters. Thus, we conclude that the luciferase substrate can enter the cells, and the intracellular reporter is suitable for further adaptation.

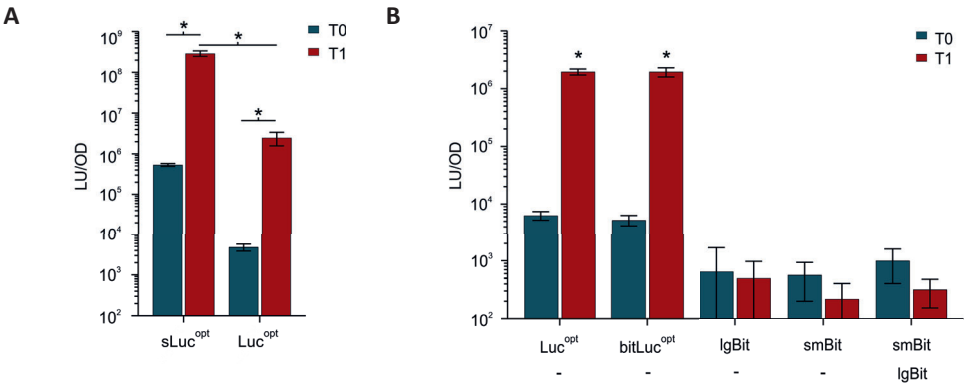


**Fig. SM2 - Controls for the split luciferase (bitLuc$^{opt}$) complementation assay.** Cells were induced with 200 ng/mL ATc for 60 min. Optical density-normalized luciferase activity (LU/OD) is shown right before induction (T0, blue bars) and 1 hour after induction (T1, red bars). The averages of biological triplicate measurements are shown, with error bars indicating the standard deviation from the mean. **A)** Luciferase activity of AP34 (P$_{tet}$-sluc$^{opt}$; extracellular luciferase) versus AP181 (P$_{tet}$-*luc*$^{opt}$; intracellular luciferase) **B)** bitLuc$^{opt}$ controls. Induction of AP181 (P$_{tet}$-*luc*$^{opt}$), AP182 (P$_{tet}$-*bitluc*$^{opt}$), AP199 (P$_{tet}$-*lgbit*), AP201 (P$_{tet}$-*smbit*) and AP202 (P$_{tet}$-*smbit/lgbit*). Interaction was defined based on the negative controls as a luciferase activity of >1000 LU/OD. Significant differences between all the values are represented * p<0,0001 by two-way ANOVA.

## References


1 Lawson, P. A., Citron, D. M., Tyrrell, K. L. & Finegold, S. M. Reclassification of Clostridium difficile as *Clostridioides difficile* (Hall and O'Toole 1935) Prevot 1938. *Anaerobe* **40**, 95-99 (2016).

2 Hensgens, M. P. *et al. Clostridium difficile* infection in the community: a zoonotic disease? *Clin. Microbiol. Infect.* **18**, 635-645 (2012).

3 Warriner, K., Xu, C., Habash, M., Sultan, S. & Weese, S. J. Dissemination of *Clostridium difficile* in food and the environment: Significant sources of C. difficile community-acquired infection? *J Appl Microbiol* **122**, 542-553 (2017).

4 Smits, W. K., Lyras, D., Lacy, D. B., Wilcox, M. H. & Kuijper, E. J. *Clostridium difficile* infection. *Nature Reviews Disease Primers* **2**, 16020 (2016).

5 Crobach, M. J. T. *et al.* Understanding *Clostridium difficile* Colonization. *Clinical microbiology reviews* **31** (2018).

6 Pituch, H. *Clostridium difficile* is no longer just a nosocomial infection or an infection of adults. *International journal of antimicrobial agents* **33 Suppl 1**, S42-45 (2009).

7 Spigaglia, P. Recent advances in the understanding of antibiotic resistance in *Clostridium difficile* infection. *Ther Adv Infect Dis* **3**, 23-42 (2016).

8 Peng, Z. *et al.* Update on Antimicrobial Resistance in *Clostridium difficile*: Resistance Mechanisms and Antimicrobial Susceptibility Testing. *Journal of clinical microbiology* **55**, 1998-2008 (2017).

9 Ehmann, D. E. & Lahiri, S. D. Novel compounds targeting bacterial DNA topoisomerase/DNA gyrase. *Curr Opin Pharmacol* **18**, 76-83 (2014).

10 Bhowmick, T. *et al.* Targeting *Mycobacterium tuberculosis* nucleoid-associated protein HU with structure-based inhibitors. *Nature communications* **5**, 4124 (2014).

11 van Eijk, E., Wittekoek, B., Kuijper, E. J. & Smits, W. K. DNA replication proteins as potential targets for antimicrobials in drug-resistant bacterial pathogens. *J Antimicrob Chemother* **72**, 1275-1284 (2017).

12 Wang, J. C. Cellular roles of DNA topoisomerases: a molecular perspective. *Nat Rev Mol Cell Biol* **3**, 430-440 (2002).

13 Pelletier, J. *et al.* Physical manipulation of the *Escherichia coli* chromosome reveals its soft nature. *Proceedings of the National Academy of Sciences of the United States of America* **109**, E2649-2656 (2012).

14 Zimmerman, S. B. & Murphy, L. D. Macromolecular crowding and the mandatory condensation of DNA in bacteria. *FEBS Lett* **390**, 245-248 (1996).

15 Dame, R. T. & Tark-Dame, M. Bacterial chromatin: converging views at different scales. *Current Opinion in Cell Biology* **40**, 60-65 (2016).

16 Dillon, S. C. & Dorman, C. J. Bacterial nucleoid-associated proteins, nucleoid structure and gene expression. *Nat Rev Microbiol* **8**, 185-195 (2010).

17 Ohniwa, R. L., Ushijima, Y., Saito, S. & Morikawa, K. Proteomic analyses of nucleoid-associated proteins in *Escherichia coli*, *Pseudomonas aeruginosa*, *Bacillus subtilis*, and *Staphylococcus aureus*. *PloS one* **6**, e19172 (2011).

18 Grove, A. Functional evolution of bacterial histone-like HU proteins. *Curr Issues Mol Biol* **13**, 1-12 (2011).

19 Kamashev, D. *et al.* Comparison of histone-like HU protein DNA-binding properties and HU/IHF protein sequence alignment. *PloS one* **12**, e0188037 (2017).

20 Boubrik, F., Bonnefoy, E. & Rouviere-Yaniv, J. HU and IHF: similarities and differences. In *Escherichia coli*, the lack of HU is not compensated for by IHF. *Res Microbiol* **142**, 239-247 (1991).

21 Claret, L. & Rouviere-Yaniv, J. Variation in HU composition during growth of *Escherichia coli*: the heterodimer is required for long term survival. *Journal of molecular biology* **273**, 93-104 (1997).

22 Guo, F. & Adhya, S. Spiral structure of *Escherichia coli* HUalphabeta provides foundation for DNA supercoiling. *Proceedings of the National Academy of Sciences of the United States of America* **104**, 4309-4314 (2007).

**23** Kohler, P. & Marahiel, M. A. Association of the histone-like protein HBsu with the nucleoid of *Bacillus subtilis*. *J Bacteriol* **179**, 2060-2064 (1997).

**24** Giangrossi, M., Giuliodori, A. M., Gualerzi, C. O. & Pon, C. L. Selective expression of the beta-subunit of nucleoid-associated protein HU during cold shock in *Escherichia coli*. *Molecular microbiology* **44**, 205-216 (2002).

**25** Painbeni, E., Caroff, M. & Rouviere-Yaniv, J. Alterations of the outer membrane composition in *Escherichia coli* lacking the histone-like protein HU. *Proceedings of the National Academy of Sciences of the United States of America* **94**, 6712-6717 (1997).

**26** van Noort, J., Verbrugge, S., Goosen, N., Dekker, C. & Dame, R. T. Dual architectural roles of HU: formation of flexible hinges and rigid filaments. *Proceedings of the National Academy of Sciences of the United States of America* **101**, 6969-6974 (2004).

**27** Dame, R. T., Hall, M. A. & Wang, M. D. Single-molecule unzipping force analysis of HU-DNA complexes. *Chembiochem* **14**, 1954-1957 (2013).

**28** Balandina, A., Kamashev, D. & Rouviere-Yaniv, J. The bacterial histone-like protein HU specifically recognizes similar structures in all nucleic acids. DNA, RNA, and their hybrids. *J Biol Chem* **277**, 27622-27628 (2002).

**29** Grainger, D. C., Hurd, D., Goldberg, M. D. & Busby, S. J. Association of nucleoid proteins with coding and non-coding segments of the *Escherichia coli* genome. *Nucleic acids research* **34**, 4642-4652 (2006).

**30** Navarre, W. W. *et al.* Selective silencing of foreign DNA with low GC content by the H-NS protein in *Salmonella*. *Science* **313**, 236-238 (2006).

**31** Gordon, B. R. *et al.* Structural basis for recognition of AT-rich DNA by unrelated xenogeneic silencing proteins. *Proceedings of the National Academy of Sciences of the United States of America* **108**, 10690-10695 (2011).

**32** Kohler, P. & Marahiel, M. A. Mutational analysis of the nucleoid-associated protein HBsu of *Bacillus subtilis*. *Mol Gen Genet* **260**, 487-491 (1998).

**33** Bensaid, A., Almeida, A., Drlica, K. & Rouviere-Yaniv, J. Cross-talk between topoisomerase I and HU in *Escherichia coli*. *Journal of molecular biology* **256**, 292-300 (1996).

**34** Dame, R. T. & Goosen, N. HU: promoting or counteracting DNA compaction? *FEBS Lett* **529**, 151-156 (2002).

**35** Swinger, K. K., Lemberg, K. M., Zhang, Y. & Rice, P. A. Flexible DNA bending in HU-DNA cocrystal structures. *EMBO J* **22**, 3749-3760 (2003).

**36** Aki, T., Choy, H. E. & Adhya, S. Histone-like protein HU as a specific transcriptional regulator: co-factor role in repression of gal transcription by GAL repressor. *Genes to cells : devoted to molecular & cellular mechanisms* **1**, 179-188 (1996).

**37** Morales, P., Rouviere-Yaniv, J. & Dreyfus, M. The histone-like protein HU does not obstruct movement of T7 RNA polymerase in *Escherichia coli* cells but stimulates its activity. *J Bacteriol* **184**, 1565-1570 (2002).

**38** Oberto, J., Nabti, S., Jooste, V., Mignot, H. & Rouviere-Yaniv, J. The HU regulon is composed of genes responding to anaerobiosis, acid stress, high osmolarity and SOS induction. *PloS one* **4**, e4367 (2009).

**39** Priyadarshini, R. *et al.* The nucleoid-associated protein HUbeta affects global gene expression in *Porphyromonas gingivalis*. *Microbiology* **159**, 219-229 (2013).

**40** Berger, M. *et al.* Coordination of genomic structure and transcription by the main bacterial nucleoid-associated protein HU. *EMBO reports* **11**, 59-64 (2010).

**41** Lewis, D. E. A., Geanacopoulos, M. & Adhya, S. Role of HU and DNA supercoiling in transcription repression: specialized nucleoprotein repression complex at gal promoters in *Escherichia coli*. *Molecular microbiology* **31**, 451-461 (1999).

**42** Chodavarapu, S., Felczak, M. M., Yaniv, J. R. & Kaguni, J. M. *Escherichia coli* DnaA interacts with HU in initiation at the *E. coli* replication origin. *Molecular microbiology* **67**, 781-792 (2008).

**43** Jaffe, A., Vinella, D. & D'Ari, R. The *Escherichia coli* histone-like protein HU affects DNA initiation, chromosome partitioning via MukB, and cell division via MinCDE. *J Bacteriol* **179**, 3494-3499 (1997).

**44** Mangan, M. W. *et al.* Nucleoid-associated protein HU controls three regulons that coordinate virulence, response to stress and general physiology in *Salmonella enterica serovar Typhimurium*. *Microbiology* **157**, 1075-1087 (2011).

**45** Alvarez, A. & Toledo, H. The histone-like protein HU has a role in gene expression during the acid adaptation response in *Helicobacter pylori*. *Helicobacter* **22** (2017).

**46** Sakatos, A. *et al.* Posttranslational modification of a histone-like protein regulates phenotypic resistance to isoniazid in mycobacteria. *Sci Adv* **4**, eaao1478 (2018).

**47** Ferrandiz, M. J., Carreno, D., Ayora, S. & de la Campa, A. G. HU of *Streptococcus pneumoniae* Is Essential for the Preservation of DNA Supercoiling. *Front Microbiol* **9**, 493 (2018).

**48** Sebaihia, M. *et al.* The multidrug-resistant human pathogen *Clostridium difficile* has a highly mobile, mosaic genome. *Nature genetics* **38**, 779-786 (2006).

**49** Dembek, M. *et al.* High-throughput analysis of gene essentiality and sporulation in *Clostridium difficile*. *MBio* **6**, e02383 (2015).

**50** Swinger, K. K. & Rice, P. A. Structure-based analysis of HU-DNA binding. *Journal of molecular biology* **365**, 1005-1016 (2007).

**51** Kelley, L. A., Mezulis, S., Yates, C. M., Wass, M. N. & Sternberg, M. J. The Phyre2 web portal for protein modeling, prediction and analysis. *Nat Protoc* **10**, 845-858 (2015).

**52** Waterhouse, A. *et al.* SWISS-MODEL: homology modelling of protein structures and complexes. *Nucleic acids research* (2018).

**53** Kim, D. H. *et al.* beta-Arm flexibility of HU from *Staphylococcus aureus* dictates the DNA-binding and recognition mechanism. *Acta Crystallogr D Biol Crystallogr* **70**, 3273-3289 (2014).

**54** Hammel, M. *et al.* HU multimerization shift controls nucleoid compaction. *Sci Adv* **2**, e1600650 (2016).

**55** Mouw, K. W. & Rice, P. A. Shaping the *Borrelia burgdorferi* genome: crystal structure and binding properties of the DNA-bending protein Hbb. *Molecular microbiology* **63**, 1319-1330 (2007).

**56** Kamau, E., Tsihlis, N. D., Simmons, L. A. & Grove, A. Surface salt bridges modulate the DNA site size of bacterial histone-like HU proteins. *Biochem J* **390**, 49-55 (2005).

**57** Saitoh, F., Kawamura, S., Yamasaki, N., Tanaka, I. & Kimura, M. Arginine-55 in the beta-arm is essential for the activity of DNA-binding protein HU from *Bacillus stearothermophilus*. *Biosci Biotechnol Biochem* **63**, 2232-2235 (1999).

**58** Goshima, N., Kohno, K., Imamoto, F. & Kano, Y. HU-1 mutants of *Escherichia coli* deficient in DNA binding. *Gene* **96**, 141-145 (1990).

**59** Smits, W. K. & Grossman, A. D. The transcriptional regulator Rok binds A+T-rich DNA and is involved in repression of a mobile genetic element in *Bacillus subtilis*. *PLoS Genet* **6**, e1001207 (2010).

**60** Seco, E. M. & Ayora, S. *Bacillus subtilis* DNA polymerases, PolC and DnaE, are required for both leading and lagging strand synthesis in SPP1 origin-dependent DNA replication. *Nucleic acids research* **45**, 8302-8313 (2017).

**61** Dixon, A. S. *et al.* NanoLuc Complementation Reporter Optimized for Accurate Measurement of Protein Interactions in Cells. *ACS chemical biology* **11**, 400-408 (2016).

**62** Oliveira Paiva, A. M., Friggen, A. H., Hossein-Javaheri, S. & Smits, W. K. The Signal Sequence of the Abundant Extracellular Metalloprotease PPEP-1 Can Be Used to Secrete Synthetic Reporter Proteins in *Clostridium difficile*. *ACS synthetic biology* (2016).

**63** Fagan, R. P. & Fairweather, N. F. *Clostridium difficile* has two parallel and essential Sec secretion systems. *J. Biol. Chem.* **286**, 27483-27493 (2011).

**64** van Eijk, E. *et al.* Complete genome sequence of the *Clostridium difficile* laboratory strain 630Deltaerm reveals differences from strain 630, including translocation of the mobile element CTn5. *BMC Genomics* **16**, 31 (2015).

**65** Los, G. V. *et al.* HaloTag: A Novel Protein Labeling Technology for Cell Imaging and Protein Analysis. *American Chemical Society* (2010).

**66** Stagge, F., Mitronova, G. Y., Belov, V. N., Wurm, C. A. & Jakobs, S. SNAP-, CLIP- and Halo-tag labelling of budding yeast cells. *PloS one* **8**, e78745 (2013).

**67** Ke, N., Landgraf, D., Paulsson, J. & Berkmen, M. Visualization of Periplasmic and Cytoplasmic Proteins with a Self-Labeling Protein Tag. *J Bacteriol* **198**, 1035-1043 (2016).

**68** Cassona, C. P., Pereira, F., Serrano, M. & Henriques, A. O. A Fluorescent Reporter for Single Cell Analysis of Gene Expression in *Clostridium difficile*. *Methods in molecular biology* **1476**, 69-90 (2016).

**69** Buckley, A. M. *et al.* Lighting Up *Clostridium Difficile*: Reporting Gene Expression Using Fluorescent Lov Domains. *Sci Rep* **6**, 23463 (2016).

**70** Ransom, E. M., Ellermeier, C. D. & Weiss, D. S. Use of mCherry Red fluorescent protein for studies of protein localization and gene expression in *Clostridium difficile*. *Appl Environ Microbiol* **81**, 1652-1660 (2015).

**71** Wery, M., Woldringh, C. L. & Rouviere-Yaniv, J. HU-GFP and DAPI co-localize on the *Escherichia coli* nucleoid. *Biochimie* **83**, 193-200 (2001).

**72** Holowka, J. *et al.* HupB Is a Bacterial Nucleoid-Associated Protein with an Indispensable Eukaryotic-Like Tail. *MBio* **8** (2017).

**73** Ransom, E. M., Williams, K. B., Weiss, D. S. & Ellermeier, C. D. Identification and characterization of a gene cluster required for proper rod shape, cell division, and pathogenesis in *Clostridium difficile*. *Journal of Bacteriology* **196**, 2290-2300 (2014).

**74** Binder, D. *et al.* Comparative Single-Cell Analysis of Different *E. coli* Expression Systems during Microfluidic Cultivation. *PloS one* **11**, e0160711 (2016).

**75** Jin, D. J., Cagliero, C. & Zhou, Y. N. Role of RNA polymerase and transcription in the organization of the bacterial nucleoid. *Chem Rev* **113**, 8662-8682 (2013).

**76** Hodges-Garcia, Y., Hagerman, P. J. & Pettijohn, D. E. DNA ring closure mediated by protein HU. *J Biol Chem* **264**, 14621-14623 (1989).

**77** Driessen, R. P. *et al.* Effect of temperature on the intrinsic flexibility of DNA and its interaction with architectural proteins. *Biochemistry* **53**, 6430-6438 (2014).

**78** van der Valk, R. A., Laurens, N. & Dame, R. T. Tethered Particle Motion Analysis of the DNA Binding Properties of Architectural Proteins. *Methods in molecular biology* **1624**, 127-143 (2017).

**79** Skoko, D., Wong, B., Johnson, R. C. & Marko, J. F. Micromechanical analysis of the binding of DNA-bending proteins HMGB1, NHP6A, and HU reveals their ability to form highly stable DNA-protein complexes. *Biochemistry* **43**, 13867-13874 (2004).

**80** Xiao, B., Johnson, R. C. & Marko, J. F. Modulation of HU-DNA interactions by salt concentration and applied force. *Nucleic acids research* **38**, 6176-6185 (2010).

**81** Lioy, V. S. *et al.* Multiscale Structuring of the *E. coli* Chromosome by Nucleoid-Associated and Condensin Proteins. *Cell* **172**, 771-783 e718 (2018).

**82** Le, T. B., Imakaev, M. V., Mirny, L. A. & Laub, M. T. High-resolution mapping of the spatial organization of a bacterial chromosome. *Science* **342**, 731-734 (2013).

**83** Sievers, F. *et al.* Fast, scalable generation of high-quality protein multiple sequence alignments using Clustal Omega. *Mol Syst Biol* **7**, 539 (2011).

**84** Jurrus, E. *et al.* Improvements to the APBS biomolecular solvation software suite. *Protein Sci* **27**, 112-128 (2018).

**85** Sambrook, J., Fritsch, E. F. & Maniatis, T. *Molecular cloning : a laboratory manual*. (Cold Spring Harbor Laboratory, 1989).

**86** Purdy, D. *et al.* Conjugative transfer of clostridial shuttle vectors from Escherichia coli to *Clostridium difficile* through circumvention of the restriction barrier. *Molecular microbiology* **46**, 439-452 (2002).

**87** Hussain, H. A., Roberts, A. P. & Mullany, P. Generation of an erythromycin-sensitive derivative of *Clostridium difficile* strain 630 (630Deltaerm) and demonstration that the conjugative transposon Tn916DeltaE enters the genome of this strain at multiple sites. *J Med Microbiol* **54**, 137-141 (2005).
**88** Driessen, R. P. *et al.* Diverse architectural properties of Sso10a proteins: Evidence for a role in chromatin compaction and organization. *Sci Rep* **6**, 29422 (2016).
**89** Gibson, D. G. Enzymatic assembly of overlapping DNA fragments. *Methods Enzymol* **498**, 349-361 (2011).
**90** Laurent, T. C. & Killander, J. A theory of gel filtration and its exeperimental verification. *Journal of Chromatography A* **14**, 317-330 (1964).
**91** Ducret, A., Quardokus, E. M. & Brun, Y. V. MicrobeJ, a tool for high throughput bacterial cell detection and quantitative analysis. *Nat Microbiol* **1**, 16077 (2016).
**92** Rueden, C. T. *et al.* ImageJ2: ImageJ for the next generation of scientific image data. *BMC Bioinformatics* **18**, 529 (2017).
**93** Fagan, R. P. & Fairweather, N. F. *Clostridium difficile* has two parallel and essential Sec secretion systems. *J Biol Chem* **286**, 27483-27493 (2011).

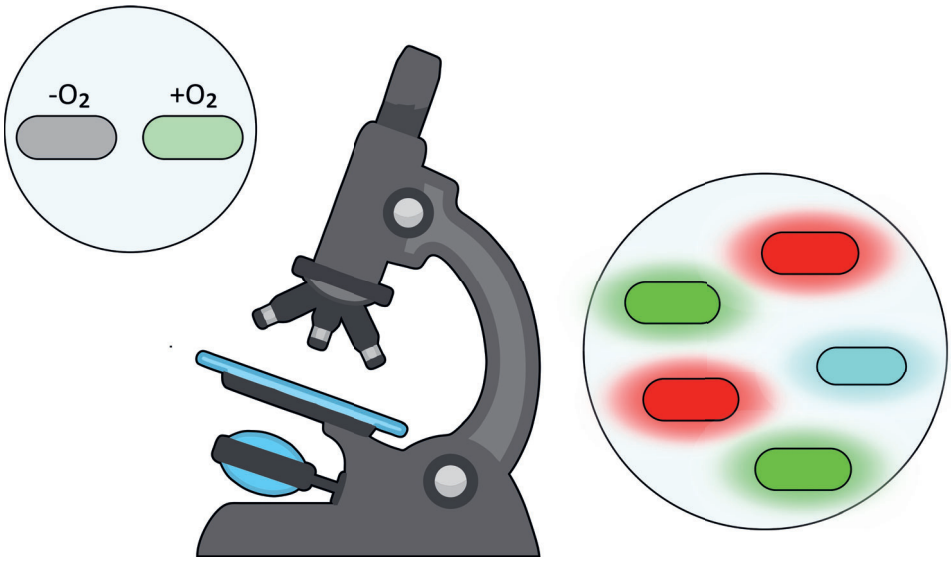
-O2
+O2